Geoderma 367 (2020) 114202

Contents lists available at ScienceDirect

Geoderma

journal homepage: www.elsevier.com/locate/geoderma

Soil temperature survey in a mountain basin

James C. Trask*, Scott M. Devine, Graham E. Fogg

Department of Land, Air, & Water Resources, University of California, Davis, CA 95616, USA

ARTICLE INFO

Handling Editor: Cristine Morgan

Keywords:
Soil temperatures
Ground-surface temperatures
Sierra Nevada
Energy balance
Physical models
Vegetation

ABSTRACT

Shallow soil temperature (*Tss*) was monitored at many clusters of sites in valley bottom areas, bordering mountain slopes, and subalpine upland areas within the Tahoe Basin of the Sierra Nevada, USA. Objectives of this survey were to: (i) accurately log *Tss* for an entire year across the panoply of ground surface environments that cover the southern Tahoe Basin area, and (ii) identify the primary factors responsible for inter-site variations in seasonal and annual mean *Tss*. The *Tss* data for snow-free and annual mean periods exhibit wider inter-site ranges than published observations for other regions, attributable to the great diversity of ground surface environments sampled. Two energy balance based models of ground surface temperature are introduced, each applicable to a wide variety of surface environments and formulated with regional calibration coefficients that can incorporate effects of seasonal snow-cover on annual mean *Tss*. The models closely fit summer monthly and annual mean *Tss* data from most sites, and confirm that the large inter-site range of shading (by vegetation and terrain) is responsible for most of the large inter-site range of observed *Tss*. Additionally, data and model results strongly suggest spatially heterogeneous soil warming rates in response to regional climate warming, and support the value of resolving spatial variations in *Tss* for groundwater flow tracing techniques.

1. Introduction

The soil temperature [*Ts*] regime is fundamental to critical zone processes; e.g. soil ecology and respiration rate, and is inter-coupled with plant community structure. Spatial variations of *Ts* across local to areal scales are coupled with land – atmosphere interactions at microclimate and larger scales, and affect patterns of subsurface water and heat flow both within and to far below the soil profile. In this article, *Ts* refers to the temperature *T* at any or all depths in the soil profile, whereas shallow soil temperature [*Tss*] refers to *T* between ground surface and circa 30 cm depth, where diurnal *T* oscillations manifest.

Maps of land surface *T* have been developed using satellite radiometric observations (e.g. Jin, 2004; Oku et al., 2006), however there is a trade-off between spatial and temporal resolution for such maps. There have been recent efforts to achieve concurrently high spatial and temporal resolutions of land surface *T* by using data from both polar-orbiting and geosynchronous satellite platforms (e.g., Quan et al., 2018). However, surface signals are obscured during cloud-cover periods; plants and snow-cover also obscure or attenuate radiation emitted by the underlying ground surface. Hence remote observations don't sample contiguous ground surface *T* in vegetated areas, or during periods of cloud or snow cover.

Most *in situ* (i.e., below ground surface) *Ts* monitoring investigations in mountain regions have been limited to a few types of sites, typically comparing forested areas with intercanopy patches (e.g. Brearshears et al., 1998; Clinton, 2003; Jimenez et al., 2007). More recently, Wundram et al. (2010) investigated *Ts* in an alpine region of central Norway, with *Ts* monitoring sites at ridges, slopes, and depressions. Over an elevation range of 0.4 km, slope, aspect, and vegetation together had a larger influence on *Ts* than did elevation, however no model for these results was mentioned. Similarly, Liu and Luo (2011) report that slope aspect and vegetation had a larger influence on seasonal and annual *Ts* than did elevation across two timberline ecotones in the Sergyemia mountains of Tibet. Liang et al. (2013) monitored summer *Ts* at ten sites in a forested mountainous area of Montana, USA. Their hybrid empirical-physical model for *Ts* includes leaf area index and soil litter parameters; however each such parameter was assigned one value for the entire study area at all times. The fine-scale spatial and temporal *Ts* heterogeneity in model output was driven entirely by corresponding fine-scale variations of air *T* (*Ta*) input. Kunkel et al. (2016) monitored *Ts* at many sites in a temperate hilly grassland region of New South Wales, Australia. Correlations of mean annual *Ts* (*Ts{an}*) data with site elevation, orientation, and soil moisture were reported, however no model of *Ts* was used to unify these observations.

The above cited and other investigations have together established that in some regions, *Ts{an}* variations exceed 3 °C across short

* Corresponding author.
E-mail addresses: jctrask1@gmail.com (J.C. Trask), smdevine@ucdavis.edu (S.M. Devine), gefogg@ucdavis.edu (G.E. Fogg).

https://doi.org/10.1016/j.geoderma.2020.114202
Received 23 December 2018; Received in revised form 28 November 2019; Accepted 17 January 2020
Available online 29 February 2020

distances within a narrow elevation band, due mainly to spatial variations of the ground surface environment, including slope, aspect, plant cover type and density, and soil moisture. However, none of these investigations addressed spatial variations of *Ts* across the full range of diverse surface environments present in many mountainous areas. In subalpine and lower elevation montane zones with warm summers and winter snow-cover, ground surface environments are often very spatially heterogeneous, consequently large spatial variability in *Ts* is expected over all time scales.

In order to capture the full range of *Tss* spatial heterogeneity, we monitored *Tss in situ* at 95 diverse sites in the southern Tahoe Basin, as described in Section 2. Two physically based models for ground temperature are introduced, each formulated using widely available surface state and exposure parameters that together can characterize a large variety of ground surface environments. Section 3 presents observations and statistics of the *Tss* data across the numerous sites monitored, including a focus on effects of snow-cover. Section 4 presents *Tss* model results, including calibration, summer monthly and annual mean simulated *Tss*, and analyses of model performance. Section 5 assesses the data and models, and presents two implications of observational and model results. Section 6 summarizes and concludes.

2. Study area and methods

2.1. Study area description

The Tahoe Basin is a 1317 km^2 mountainous basin in the central eastern Sierra Nevada of California and Nevada, USA (Fig. 1). Elevations range from 1.90 km at the Lake Tahoe shoreline to 3.32 km at Freel Peak. About half the basin land area has slopes >20% (Crippen and Pavelka, 1970) at all aspects; in contrast several large valley bottom areas are nearly flat (slope <3%). The study area is a ~150 km^2 portion of the Tahoe Basin south of Lake Tahoe (Fig. 1). This area was selected for a *Ts* survey to aid in related field investigations of Tahoe subsurface heat and groundwater flow (Trask and Fogg, 2009).

Granitic bedrock underlies the study area. There are large areas of exposed granite on slopes and upland areas, dominated by glacially scoured, lightly weathered (and sparsely vegetated) bedrock on the western side and deeply weathered sandy gruus near the eastern study area edge. Upland depressions and lowland valleys have accumulated glacial, alluvial, and lacustrine deposits (Birkeland, 1964). The pattern of soil types is complex (USDA and NRCS, 2007). Soil erosion and movement has occurred in many areas; soil depths range from thin veneers in upland areas to deposits several feet deep in some valley areas.

The Tahoe Basin has a montane Mediterranean climate. Isohyetal maps (e.g. Crippen and Pavelka, 1970; Thodal, 1997) illustrate mean annual precipitation ranges from ~60 cm/yr at low elevations in the northeast of the study area to ~150 cm/yr at high elevations near the southern and western boundaries. Most precipitation originates from Pacific storm fronts between mid-October and late April, falling mainly as snow. Snow pack typically persists thru late April at low elevations and into June at high elevations. Mean annual *Ta* (*Ta{an}*) was ~6.0 °C over the period 1968–2007 at the Tahoe Valley Airport (location Fig. 1).

Within the study area are many areas and patches of conifer forest, chaparral, meadow, and sparsely vegetated soil or exposed rock (Crippen and Pavelka, 1970, and our field observations), as is common in montane and sub-alpine zones throughout the Sierra Nevada. Conifer forest areas are typically dense, consisting mainly of pine and fir species. Chaparral consists largely of manzanita and other brush, of widely varying height and density. In lightly forested areas there is often a mix of conifers and chaparral. Open meadows occupy many flat areas in both lowland valleys and uplands, dominated by grasses and herbage. Wet meadows over shallow water tables are lush and green throughout summer; other meadows dry out during summer with browning and wilting of vegetation.

2.2. Soil temperature monitoring sites and probe deployment

Probes for *Tss* monitoring were deployed at 99 soil sites in the study area. Fig. 1 shows the locations of the 95 sites where *Tss* data were recovered. At most sites, monitoring initiated during summer 2004 and was terminated Oct. 2005. Monitoring was extended until fall 2006 or 2007 at twelve sites. At each site *Tss* was logged at 30-minute intervals to capture diurnal oscillations and enable determination of 24-hr mean *Tss*. Monitoring sites were located across the following types and ranges of surface environmental characteristics:

- Local slope of ground surface: flat to ~40°
- Local aspect of ground surface: N, NE, E, SE, S, SW, W, NW, or minor aspects
- Elevation of ground surface: 1.91 km near Lake Tahoe to 2.32 km (see Fig. 1)
- Vegetation: each major class (see Section 2.1 above), very sparse to dense coverage
- Ground surface material: soil with or without litter cover, or exposed granitic bedrock
- Ground surface color: light to dark hued, many colors
- Shallow soil moisture during summer dry season: very dry to nearly saturated

Most sites were part of a cluster, wherein several probes were located close to each other (Fig. 1) with differing ground surface meteorologic exposure (first four bullet points above) and/or surface state conditions (last three bullet points) at each site in a cluster. Table S1–2 in Supplement 1F lists ground surface exposure and state parameter values at each site.

Robust, inexpensive probes with built-in automated *T* logging ('Hobo Water Temp Pro', Onset Corp.) were used for *Tss* monitoring. Calibration checks over the range 0–30 °C were performed on most probes both before and after field deployment; all probes tested were stably accurate to within +/− 0.15 °C across their deployment periods.

At each soil site one probe was buried, with the sensing element at 15 (+/−1) cm depth below ground surface. This depth is a compromise between being shallow enough to ensure clearly discernable diurnal *T* oscillations, and deep enough so that effects of micro-scale ground surface spatial environmental heterogeneities on soil *T* are averaged out. There was minimal disturbance to the overlying ground surface cover during probe burial and data retrieval. Supplement 1A further describes the soil *T* probe and its calibration and deployment, and supplement 1B includes photographs of several *Tss* monitoring sites.

2.3. Ground surface energy balance and temperature models

2.3.1. Formulation of energy balance and temperature models

For a thin ground surface layer (i.e. negligibly small thermal energy storage capacity), conservation of energy entails that the net radiative energy transferred to ground surface is balanced by net non-radiative transfers of energy away from ground surface; formulated as

$$(1-\alpha)\cdot Ri\{f, r, z\} + \varepsilon_g\cdot[\varepsilon_{sv}\{f\}\cdot\sigma_B\cdot Ta\{z\}^4] - \varepsilon_g\cdot[\sigma_B\cdot(Tgs - C0)^4] = LE + h_c\{f, Va\}\cdot(Tgs - Ta\{z\} - C0) - C1 \quad (1)$$

where α = ground surface albedo ($0 < \alpha < 1$), *Ri {f, r, z}* = solar insolation incident at ground surface (flux), ε_g = ground surface thermal (long-wave) emissivity ($0 < \varepsilon_g < 1$), ε_{sv}{f} = sky-view thermal (long-wave) emissivity ($0 < \varepsilon_{sv} < 1$), σ_B = Stefan-Boltzmann constant = 5.67×10^{-8} W m^{-2} K^{-4}, *Ta{z}* = air temperature at a reference height above ground surface (°K), *Tgs* = ground surface temperature (°K), *LE* = latent heat loss from the ground surface and

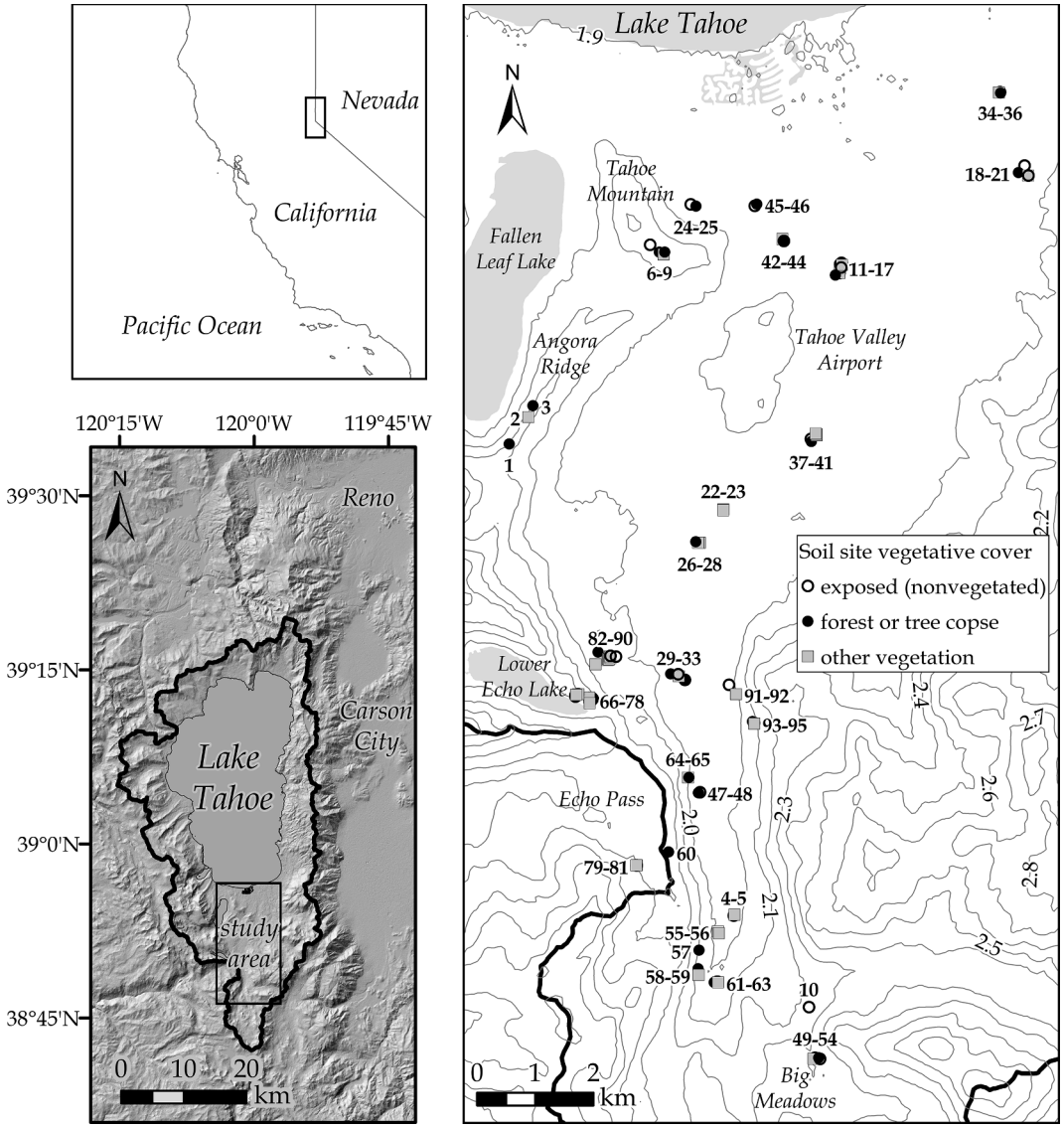

Fig. 1. Location of Tahoe Basin (top left map) and study area (bottom left map). The study area detail map (right) shows elevation *z* contour lines spaced at 0.10 km intervals and the shallow soil temperature (*Tss*) monitoring site locations (labeled from 1 to 95).

shallow soil (flux), h_c *{f, Va}* = convective (sensible) heat transfer coefficient (flux/°K), and *C0, C1* = time-dependent coefficients (*C0* units °K, *C1* units flux). Also, f = fraction of site shading by vegetation and terrain ($0 < f < 1$), z = site elevation, r = site orientation (i.e., local slope S and aspect), and Va = wind speed. Units of Eq. (1) are energy flux (energy/time/area). The first two terms on the left side of Eq. (1) represent solar and thermal radiation absorbed by the ground surface, the third term approximates thermal radiation emitted from ground surface. This net radiation input is balanced by energy outputs on the right side of Eq. (1), including latent heat loss due to evaporation E from the ground (excluding transpiration and sublimation), and convective (sensible) heat transfer between the ground surface and atmosphere (which can be positive or negative). In Eq. (1), *C1* incorporates conductive heat flow between the ground surface and subsurface, which varies with the amplitudes and phases of the diurnal and annual *Tgs* oscillations. When applying this energy balance formulation to a variety of surface environments in a geographic region, then together with *C0*, *C1* can function as a calibratable regional correction factor, as detailed later.

The term $(Tgs\text{-}C0)^4$ in Eq. (1) is linearized in *Tgs* using the identity $Tgs - CO = Ta\{z\} + \Delta T$ where $\Delta T = (Tgs - Ta\{z\} - CO)$, and the approximation $(T + \Delta T)^n \approx T^n + nT^{n-1}\Delta T$ for $\Delta T/T << 1$. Substituting $(Tgs - CO)^4 \approx (Ta\{z\})^4 + 4(Ta\{z\})^3 \cdot (Tgs - Ta\{z\} - CO)$ into Eq. (1) and solving for *Tgs*;

$$Tgs = Ta\{z\} + CO + [C1 - LE + (1 - \alpha)\cdot Ri\{f, r, z\} + \sigma_B \varepsilon_g \cdot (\varepsilon_{sv}\{f\} - 1)\cdot (Ta\{z\})^4]/[h_c\{f, Va\} + 4\sigma_B \varepsilon_g \cdot (Ta\{z\})^3] \quad (2)$$

For the quotient in Eq. (2), terms in the numerator have energy flux units and terms in the denominator have units energy flux/°K. Important determinants of values of terms include *f*, *r*, *z*, *Va*; explicit approximate functional dependences on *f*, *r*, *z* are described below.

Many model forms for h_c have been used in published reports of the ground surface energy balance, most of which are not parameterized for vegetative sheltering, and yielding a wide range of estimated values for ground surface h_c (e.g., Ouzzane et al., 2014). The simple formulation below accounts for vegetative sheltering and is calibratable:

$$h_c\{f, Va\} = (1 - 0.44f)\cdot C_h \quad (3)$$

where the factor (1–0.44*f*) is similar to a vegetation factor used by Herb et al. (2008) to account for reduction of h_c under vegetation (see Supplement 1C), and $C_h = C_h\{Va_{ex}\}$ where Va_{ex} is wind speed at a non-vegetated (exposed) location with large fetch. For simplicity, C_h is

modeled to have the same value at all sites (but changes over time as Va_{ex} changes). A regional value of C_h at a specified time can be estimated by calibration, as described later.

$Ta\{z\}$ is modeled with linear z lapse:

$$Ta\{z\} = Ta_0 - L_a \cdot \Delta z \tag{4}$$

where $Ta_0 = Ta$ measured at reference elevation zo, L_a = areal Ta lapse rate (at 2-m height above land surface; units °C/km) and $\Delta z = z - zo$ (units km). $Ri\{f,r,z\}$ is modeled as follows:

$$Ri\{f, r, z\} = (1 - f) \cdot Rc\{r, z\} \tag{5}$$

$$Rc\{r, z\} = Rc_0 \cdot [\exp(L_R \cdot \Delta z)] \cdot Rn_0(r) \tag{6}$$

where $Rc\{r,z\}$ = over-canopy solar radiation, Rc_0 = solar radiation incident on an exposed level surface ($S = 0°$) at $z = zo$, L_R is z lapse of solar radiation ($L_R > 0$), and $Rn_o\{r\}$ is normed over-canopy radiation at $z = zo$, i.e. $Rn_0\{r\} = Rc\{r, zo\}/Rc_0$ (dimensionless), with $Rn_o\{r\} = 1$ for a level surface. The L_R term adjusts for the increase in solar radiation flux transmitted thru the atmosphere to land surface as z increases (e.g. Coops et al., 2000; Allen et al., 2006).

Long-wave radiation incident on the ground surface is sourced from the atmosphere (air and clouds) of emissivity ε_{atm}, vegetation canopy near the site of emissivity ε_{can}, and site-facing terrain of emissivity ε_{ter}. Approximations for ε_{sv} and ε_{atm} are:

$$\varepsilon_{sv} \approx (1 - F_{sky}) \cdot \varepsilon_{ter} + F_{sky} \cdot [0.55f \cdot \varepsilon_{can} + (1 - 0.55f) \cdot \varepsilon_{atm}] \tag{7}$$

$$\varepsilon_{atm} \approx 1.72(e_a\{z\}/Ta\{z\})^{1/7} \cdot (1 + 0.22F_C^2) \tag{8}$$

where $F_{sky} = 1 - (S/180°)$, $e_a\{z\}$ = vapor pressure (kPa), $Ta\{z\}$ units are °K, and F_C = fractional cloud cover. Eq. (7) is revised from Dingman (2002) by replacing f with $0.55f$ (see Supplement 1C). For Eq. (8), a relation $\varepsilon_{atm} = 1.72(e_a/Ta)^{1/7}$ is from Brutsaert (1975) for clear sky conditions; the cloud cover factor $(1 + 0.22F_C^2)$ is from Kustas et al. (1994).

Eqs. (3) and (5) are substituted into Eq. (2) to yield final form regression equations for Tgs at any snow-free (sf) time and for temporal mean Tgs over an annual (an) time period:

$$\begin{aligned} Tgs\{sf\} = {} & Ta\{z\} + (C_{LO} \cdot \Delta z) + [C1' - LE' + (1 - \alpha)(1 - f)Rc'\{r, z\} + \\ & \varepsilon_g(\varepsilon_{sv}\{f\} - 1)(Ta\{z\})^4/(4Ta_O^3)] \\ & /[C_h'(1 - 0.44f) + \varepsilon_g(Ta\{z\}/Ta_O)^3] \end{aligned} \tag{9}$$

$$\begin{aligned} Tgs\{an\} = {} & Ta\{z\} + (C_{LO} \cdot \Delta z) + CO + [\exp(C_{Lr} \cdot \Delta z)] \cdot \\ & [-LE' + (1 - \alpha)(1 - f)Rc'\{r, z\} + \varepsilon_g(\varepsilon_{sv}\{f\} - 1)(Ta\{z\})^4/(4Ta_O^3)] \\ & /[C'_h(1 - 0.44f) + \varepsilon_g(Ta\{z\}/Ta_O)^3] \end{aligned} \tag{10}$$

Primed variables in Eqs. (9), (10) are equal to unprimed variables in Eq. (2) divided by $4 \cdot \sigma_B \cdot Ta_O^3$; resulting terms in the numerators of Eqs. (9), (10) have units °K and terms in the denominator are dimensionless. For snow-free periods $C0$ from Eq. (2) is set to zero, whereas for annual periods $C1$ from Eq. (2) is set to zero. Lapse terms $(C_{LO} * \Delta z)$ and exp $(C_{Lr} * \Delta z)$ are introduced in Eqs. (9), (10), with lapse coefficients C_{LO}, C_{Lr} accounting for z lapse of Tgs in addition to that imparted by the numerical estimates of L_a, L_R in Eqs. (4), (6). Section 4.4.1 and Supplement 3 explain the particular placement of C_{LO} and C_{Lr} within Eqs. (9), (10).

Numerical values of each of the Ci coefficients in Eqs. (9) or (10) are determined by regression of model Eqs. (9) or (10) against temperature data from many sites for a common specified time or time period (one instantaneous or temporal-mean datum per site). Expressions (4), (6), (7), (8) are substituted into Eqs. (9), (10) for regression.

2.3.2. Applicability to shallow soils

Model Eqs. (9) and (10) are derived for ground surface temperature Tgs, but field measurements available to calibrate the models are of shallow soil temperature Tss at 15 cm depth. At any instant, Tss can differ substantially from overlying Tgs due to temporal lag of changes in Tss behind changes in Tgs. The shallow soil effective thermal diffusivity κ governs the rate of conduction of temporal changes of Tgs downward into the soil profile. The value of κ is a function of soil composition, and changes with time at all locations due to the marked dependence of κ on soil moisture content (e.g., Jury et al., 1991).

However, time-average Tss closely approaches time-average Tgs for sufficiently long averaging periods τ. Analyses (Supplement 2B) indicate that during the snow-free season, for time intervals during which daily changes in 24-hr mean Tgs approximate those of a model fit sinusoidal oscillation of period ~ 1 year, a minimum τ of 24 h (at depths between ~ 2 cm and ~ 30 cm) is needed for $Tss\{\tau\}$ to closely approach $Tgs\{\tau\}$. When 24-hr mean Tgs has inter-daily changes that rise (or fall) more steeply than this model oscillation, then multi-day τ may be needed; τ as long as ~ 15–30 days may be required if there are large abrupt changes in Tgs (e.g., upon spring snowmelt completion) during or shortly prior to the averaging period, in order to ensure that $Tss\{\tau\}$ at 15 cm depth closely approaches $Tgs\{\tau\}$. The Ci coefficients in Eq. (9) (when calibrated) incorporate and offset most of the site-mean discrepancy between $Tss\{\tau\}$ and $Tgs\{\tau\}$ (Section 5.2.1). Thus Eq. (9) can be used to model Tss for integer-day averaging periods during the snow-free warm season.

Previous investigations in other areas have shown that $Tss\{an\}$ varies only slightly, at most, with depth in the soil profile (West, 1952; Baxter, 1997; Rajver et al., 2006; Garcia-Suarez and Butler, 2006; Oliva et al., 2014), except where there is seasonal soil freezing or permafrost, where $Tss\{an\}$ may decrease with depth (Goodrich, 1982; Wundram et al., 2010). That is, for non-freezing soils $Tss\{an\} \sim Tgs\{an\}$ and Eq. (10) can also be used for $Tss\{an\}$.

2.3.3. Values of model terms and parameters for the Tahoe soil sites

Values of all terms on the right sides of Eqs (9), (10) except the Ci are determined using data and estimates. Many parameter values are time-dependent and/or site-specific (i.e., vary spatially). Table 1 lists the many sources of data and estimates for model terms and parameters, and their WY 2005 summer and annual values or site statistics. Error in the L_a estimate does not significantly affect fits of model Eqs. (9), (10) to data, since the calibration term $(C_{LO} \cdot \Delta z)$ compensates for such error. Estimates of insolation include direct beam, diffuse, and terrain-reflected components. Mean annual α and ε_g values have been adjusted for the presence of seasonal snow-cover. $LE = \lambda_v \cdot E$ where λ_v = latent heat of vaporization (2470 MJ/m^3) and E excludes transpiration and snow sublimation. Direct measurement-based estimates of E were not obtained; instead E has been roughly estimated for each of several site classifications. Supplement 1 includes details of site parameter estimation methods.

The 'z rank' line on Fig. 2a, b illustrates that about 2/3 of the sites are located at low elevation ($1.91 < z$ (km) < 2.08) and 1/3 at high elevation ($2.16 < z$ (km) < 2.42); no sites are located between 2.08 and 2.16 km. Fig. 2a, b illustrate that model parameter values are well-distributed across both high z and low z sites, although high z sites tend to be located on steeper slopes with a more easterly aspect than low z sites, and estimated E tends to be smaller at high z sites. High z sites have about the same distribution of f as low z sites.

3. Results 1: Observations and statistics of soil temperature data

Soil T probes from 95 sites (Fig. 1) were recovered and downloaded fall 2005. Each probe had logged Tss readings at 30 min intervals for its entire deployment period, which included summer 2005 at all 95 sites and the entire WY 2005 period at 83 of these sites.

This section presents seasonal and mean annual Tss observations, and compares Tss data among sites with respect to z, $Ta\{z\}$, vegetation, and snow-cover. The detailed descriptions in this section are not necessary for those readers primarily interested in model results

Table 1
Temperature Model Inputs: WY 2005 summer monthly and annual mean values of terms and parameters at Tahoe soil sites.

Model term or parameter		Source[a]	Unit	July 2005	August 2005	WY 2005
Symbol	Description			(n = 95)	(n = 95)	(n = 83)
Ta_o	air T at $z = z_o$	Tahoe airport data	°C	17.58	15.83	5.85
L_a	air T lapse	initial estimate	°C/km	6.0	6.0	6.0
Rc_o	[b]solar flux at $z = zo$	prior Tahoe data	MJ/m^2-day	25.75	23.95	17.46
L_R	solar flux lapse	estimate	km^{-1}	0.0953	0.0953	0.0953
F_c	fraction cloud cover	estimate	–	0.20	0.20	0.447
e_{a0}	vapor pressure at $z = z_o$	prior Tahoe data	kPa	0.917	0.908	0.571
ε_{atm}	atm. emissivity	Eq. (8)	–	0.762	0.762	0.741
ε_{can}	canopy emissivity	estimate	–	0.96	0.96	0.96
ε_{ter}	terrain emissivity	estimate	–	0.94	0.94	0.948
z	elevation	measured (GPS)	km	1.911 [2.059] 2.318	1.911 [2.059] 2.318	1.912 [2.077] 2.318
S	slope	measured (clinometer)	degrees	0.0 [9.8] 40	0.0 [9.8] 40	0.0 [10.7] 40
–	aspect	measured (compass)	degrees	N, NE, E, SE, S, SW, W, NW	N, NE, E, SE, S, SW, W, NW	N, NE, E, SE, S, SW, W, NW
$Rn_o\{r\}$	[b]normalized solar flux	computed	–	0.832 [0.980] 1.000	0.768 [0.981] 1.026	0.690 [0.981] 1.095
–	[c]ground surface color	visual observation	–	many	many	many
α	ground surface albedo	estimated from color	–	0.15 [0.304] 0.40	0.15 [0.304] 0.40	0.285 [0.398] 0.46
ε_g	ground surface emissivity	estimated from α	–	0.867 [0.899] 0.950	0.867 [0.899] 0.950	0.904 [0.922] 0.954
ε_{sv}	skyview emissivity	Eq. (7)	–	0.776 [0.828] 0.871	0.776 [0.828] 0.871	0.757 [0.813] 0.864
f	fraction shading	visual observation	–	0.050 [0.544] 0.90	0.050 [0.544] 0.90	0.050 [0.525] 0.88
E	ground surface evap.	estimated	cm	0.2 [0.73] 1.4	0.4 [1.22] 1.8	2.0 [13.8] 20

Top half of table lists site-invariant terms; bottom half of table lists site-specific terms (values minimum [mean] maximum among the n sites).
[a] Supplement 1 details sources of data and estimates; Table S1–2 lists values of model terms and parameters at each site. note: z_o = 1.92 km, 'measured' denotes measured at site by co-author James Trask, 'visual observation' at site by James Trask.
[b] Over-canopy: Rc_o on level surface (i.e., zero slope) and $Rn_o(r)$ for surface orientation r (defined by S and aspect).
[c] Colors observed: brown, red, green, grey, white, black (also mixtures of these colors and light to dark hues).

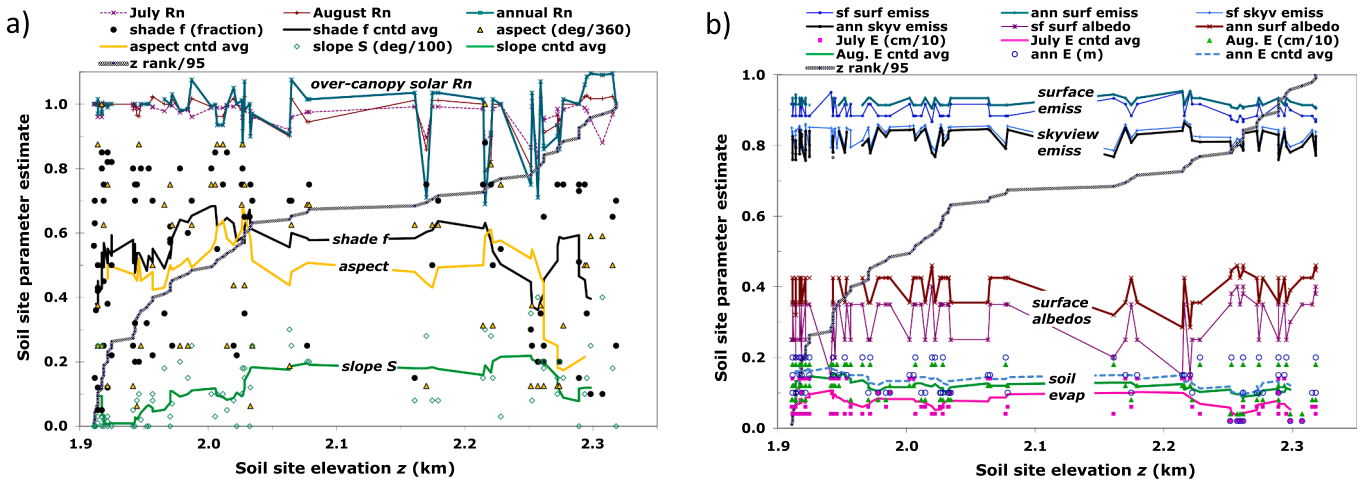

Fig. 2. Values of site-dependent soil T model input terms and parameters for each of the 95 soil sites. In a), $Rn = Rn_o\{r\}$, and aspect is measured in degrees clockwise from North. In a) and b), 'z rank' is the number of soil sites located at or below z. For b), 'sf' = snow-free, 'surf' = surface, 'emiss' = emissivity, 'ann' = annual, 'skyv' = skyview. 9-point centered average lines are shown in a) for f, aspect, S, and in b) for E.

(Section 4). Each site is put into a vegetative cover class: tree copse or forest ($0.7 < f < 0.9$), lone tree (in exposed area or meadow), brush, grass, exposed soil (little or no vegetation in immediate vicinity of site; $0.05 < f < 0.5$), lush (wet or damp soil throughout summer and early fall due to very shallow water table), and exposed litter (exposed site with litter cover > 2 cm thick). For $Ta\{z\}$ graphed in Figs. 3–7, all Ta_o data are from the Tahoe Valley Airport and L_a values are revised from Table 1 as follows: for summer (and Ta_{max}) and WY 2005, L_a are 4.5 °C/km and 4.9 °C/km respectively (Section 4.4.1); L_a for Nov., Dec, and Jan. are 4.9, 3.9, and 4.4 °C/km, respectively (Dobrowski et al., 2009).

Table 2 lists descriptive statistics of temporal mean Tss data and ($Tss - Ta\{z\}$) among all monitored sites for each of several time periods, showing inter-site ranges are broad, skews small, and kurtoses near normal. Table S1–3 in Supplement 1F lists Tss data from each site.

3.1. Winter and spring snow-cover and snow-melt periods

Snow-cover is indicated by the absence of diurnal variations in Tss. Tss data indicate that snow-cover was present at nearly all sites during nearly all days from Nov. 2004 thru April 2005 (and some days in late Oct. and May, and into early June at some high z sites).

Under snow-cover, Tss were near 0 °C (e.g. Fig. 3a). Minimum 24-hr mean Tss (Tss_{min}) during WY 2005 were between −1.35 °C and + 1.55 °C at all but two sites (Fig. 4a) with a mean site value

Table 2
Statistics of temporal mean Tahoe *Tss* data (top half of table) and of (*Tss–Ta{z}*) values (bottom half of table) for WY 2005.

Tss or (*Tss-Ta*) quantity	*n*	Min. (°C)	Max. (°C)	Rge (°C)	Median (°C)	Mean (°C)	σ (°C)	Rge/2σ (–)	Skew (–)	Kurtosis (–)
Tss_{min}	88	−1.88	+2.30	4.18	+0.27	+0.26	0.62	3.37	−0.21	**+2.31**
Tss_{max}	95	11.36	30.30	18.94	18.31	19.61	5.01	1.89	+0.47	−0.94
Tss_{max}–Tss_{min}	88	11.12	30.61	19.49	18.20	19.43	5.27	1.85	+0.43	−0.93
(Tss_{max} + Tss_{min})/2	88	5.80	15.00	9.20	9.52	9.98	2.42	1.90	+0.41	−0.93
Tss{July}	95	9.59	27.41	17.83	16.66	17.75	4.65	1.92	+0.43	−0.95
Tss{Aug.}	95	9.60	26.60	17.00	16.28	17.32	4.15	2.05	+0.44	−0.82
Tss{an}	83	3.86	12.49	8.64	6.58	6.92	1.57	2.75	**+1.08**	**+1.80**
[a]*Tss{an}* (exclude ES sites)	81	3.86	11.33	7.47	6.49	6.80	1.38	2.71	**+0.69**	+0.81
Tss_{min}–Ta_{min}{z}	88	8.81	13.69	4.88	11.70	11.70	0.96	2.54	−0.31	−0.05
Tss_{max}–Ta_{max}{z}	95	−8.37	10.09	18.46	−2.14	−1.15	5.07	1.82	**+0.52**	−0.87
Tss{July}–Ta{July, z}	95	−6.33	10.99	17.32	−0.07	0.79	4.70	1.84	+0.49	−0.88
Tss{Aug.}–Ta{Aug., z}	95	−4.57	12.10	16.67	1.01	2.11	4.21	1.98	+0.47	−0.82
Tss{an}–Ta{an, z}	83	−0.48	8.50	8.98	1.62	1.84	1.57	2.86	**+1.46**	**+3.99**
[a]*Tss{an}–Ta{an, z}* (exclude ES sites)	81	−0.48	5.44	5.92	1.60	1.69	1.27	2.33	+0.43	−0.07

n = # Tahoe soil monitoring sites for which *Tss* data are included for statistics (=all sites with available *Tss* data).
Min. = minimum 24-h mean, max. = maximum 24-hr mean, rge = range (i.e., max.–min.); (–) = dimensionless.
σ = standard deviation, kurtosis is the kurtosis in excess of that for a normal distribution.
Ta{z} from Eq. (4) with L_a values: Nov. 2004 (min. *Ta*) 4.9 °C/km; summer 2005 4.5 °C/km, WY 2005 4.9 °C/km.
For a normal distribution with *n* = 81 (95) the expected value of range/2σ is 2.26 (2.31).
Bold font values for skew and kurtosis are those values that differ from that for a normal distribution by > 2 std. errors.
For a normal distribution with *n* = 81 (95) the standard error of (i) skew is ~ 0.27 (0.25), (ii) kurtosis is ~ 0.54 (0.50).
[a] Statistics on this line exclude data from the two outlier 'Echo slide' sites (see Fig. 6c).

of + 0.26 °C+/-0.62 °C (1σ). Fig. 3a shows Tss_{min} at forested sites were on average ~ 0.4 °C warmer than at exposed sites. Tss_{min} at exposed sites were between −1.1 to + 0.8 °C; the coldest Tss_{min} was at a low *z* site under a tree (-1.9 °C), and the warmest at a lushly vegetated site near a perennial spring (+2.3 °C). At most sites with Tss_{min} > 0 °C, the minimum occurred during the April-June snowmelt period, suggesting infiltration of melt-water resulted in additional soil cooling at these sites.

During WY 2005, Ta_{min} (minimum 24-hr mean *Ta*) was −10.7 °C at the airport. At all the soil sites $Tss_{min} \gg Ta_{min}$ and Tss_{min} were also warmer than Dec. and Jan. monthly mean *Ta{z}* (Fig. 4a). Fig. 4a illustrates there is no trend of decrease of Tss_{min} with increasing *z* across the 0.41 km *z* range of sites. The insulating influence of seasonal snow-cover on *Tss* increases rapidly as snow depth increases from 0 to ~ 40 cm, and then more slowly as snow-cover approaches ~ 1 m depth (Zhang, 2005; Maurer and Bowling, 2014). NRCS SNOTEL data for WY 2005 from two stations near the western edge of the study area indicate that snow-cover was deeper than 40 cm from late Dec. to mid-April at *z* = 1.90 km, and from late Oct. to early June at *z* = 2.33 km. Snow-cover was deeper than 100 cm for only ~ 10 days in mid-Jan. at *z* = 1.90 km, but from early Dec. thru late May at *z* = 2.33 km.

At 24 of the 88 sites (27%) monitored during winter, Tss_{min} < 0 °C, including 32% (18/57) of low *z* sites and 19% (6/31) of high *z* sites. At sites with Tss_{min} < 0 °C, the minima occurred between Nov. 21 and Jan. 9, following periods of *Ta* warming and some melting of snow-cover. The duration of *Tss* < 0 °C was 1 to 12 days at 21 sites; 21 days at a high *z* site (Tss_{min} = -0.55 °C), and 39 and 47 days at two low *z* sites (Tss_{min} = -0.03 °C and −0.60 °C). Warming of *Tss* back to above 0 °C occurred under snow-cover, well before initiation of spring melt. NRCS SNOTEL data from the western edge of our study area indicate that between late Nov. and early Jan., shallow soil moisture in silty soil was between ~ 10% vol/vol and field capacity at low *z*, and ~ 2% to ~ 15% vol/vol at high *z*. This suggests that many of the 15 low *z* sites with Tss_{min} < -0.03 °C likely had an episode of early winter soil freezing; however the 6 high *z* sites with Tss_{min} < 0 °C (-1.03 °C < Tss_{min} < -0.08 °C) may not have had a soil freezing episode, due to the marked depression below 0 °C of the freezing temperature in soils with low water content (i.e., large negative matric head).

Snowmelt completion is indicated by rapid increase in *Tss* and onset of diurnal *Tss* oscillations. The *Tss* profiles in Fig. 3b show these indicators of snowmelt completion occurred in early May at two low *z* sites. Based on *Tss* observations, several sites apparently had more than one episode of snow-cover and complete melt between fall 2004 and spring 2005. Spring snow-cover duration increased with *z* by ~ 3–7 weeks over the 0.41 km *z* range of the study area. Fig. 3a shows completion of spring 2005 snowmelt occurred in mid-June at a high *z* (2.32 km) exposed site, ~5 weeks later than at a low *z* (1.94 km) exposed site. Periods of WY 2005 snow-cover and melt completion *z* dependence, as indicated by our *Tss* data, are consistent with Tahoe Basin snowpack monitoring (NRCS and NWCC, 2005).

3.2. Summer

Summer 2005 *Tss* varied widely across sites (Table 2). Fig. 3b, c illustrate that amplitudes of diurnal *Tss* oscillations were ~ 5-fold to ~ 10-fold larger at an exposed site than a dense forest site, due mainly to larger diurnal *Tgs* amplitudes and secondarily to larger κ at the exposed site (Supplement 2B). Fig. 3b also shows that 24-hr mean *Tss* fluctuates with a short lag time (~1–3 days) behind multi-day fluctuations in 24-hr mean *Ta*, and with reduced amplitude at the 15 cm sensor depth, depending on the duration of the *Ta* fluctuation and the value of κ. Fig. 3c shows that a 2.0 cm rainfall event on Aug. 15 is associated with reduction in amplitude of the Aug. 15 diurnal *Tss* oscillation at both a forested and an exposed site, and a marked cooling in 24-hr mean *Tss* from Aug. 15–17 at the exposed site (see also Fig. 3b), likely attributable to increase in cloud cover and soil *E* (Supplement 2B).

Tss_{max} (peak 24-hr mean summer 2005 *Tss*) ranged from 11.4 °C to 30.3 °C among the 95 sites, as compared to ~ 19.7 °C (*z* = 2.32 km) to 21.5 °C (*z* = 1.91 km) for Ta_{max} (i.e., peak 24-hr mean summer *Ta*, with summer L_a ~ 4.5 °C/km). During summer 2005, Tss_{max} were about 2 °C warmer than and very highly correlated with *Tss{July}* (Fig. 5a). Among all 95 sites, *Tss{July}* ranged from 9.6 °C to 27.4 °C, and *Tss{Aug.}* ranged from 9.6 °C to 26.6 °C (Fig. 6a, b). *Tss{July}* ranged among sites from 6.3 °C cooler to 11.0 °C warmer than *Ta{July}*, and *Tss{Aug.}* ranged among sites from 4.6 °C cooler to 12.1 °C warmer than *Ta{Aug.}* (using summer L_a = 4.5 °C/km). Fig. 5b shows that during July and Aug., at nearly all forest and tree-shaded sites *Tss* < *Ta{z}*; by contrast at exposed sites *Tss* > *Ta{z}*. Partially shaded brush and grass

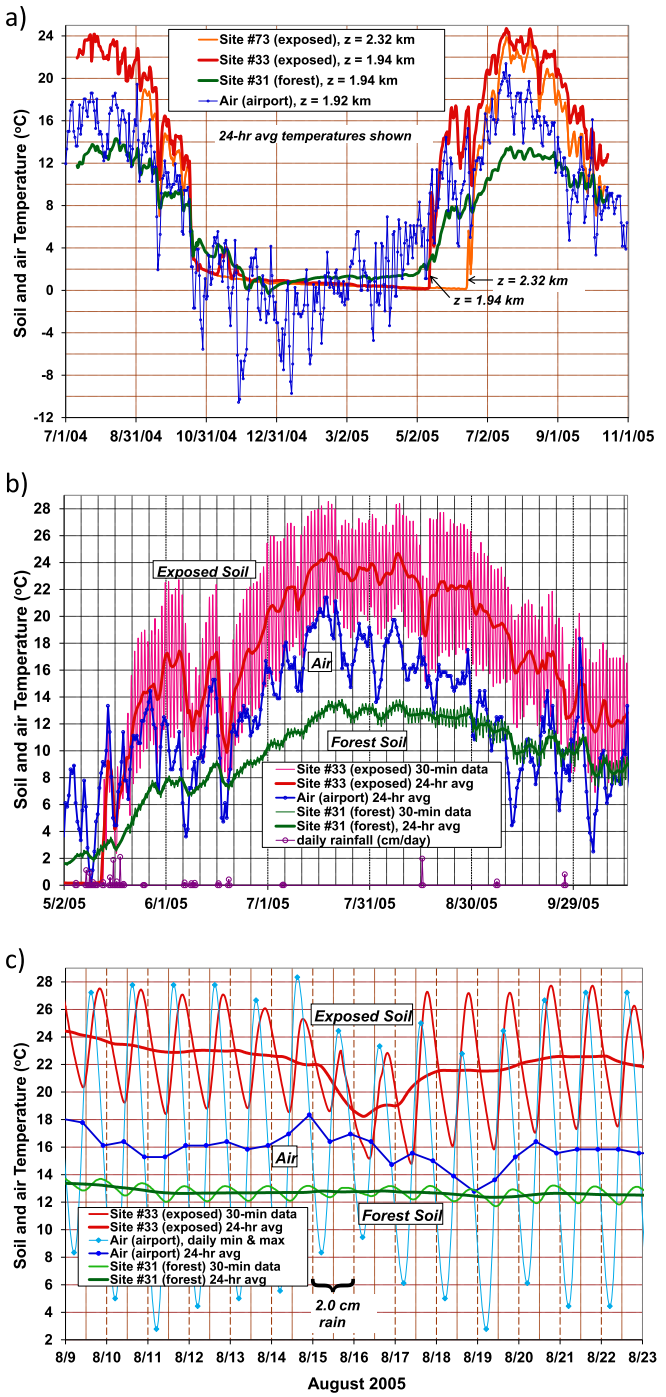

Fig. 3. Air *T* and soil *T* monitoring data from (a) exposed soil site #73 at high elevation *z* and soil sites #31 (exposed) and #33 (forested) at low *z*, from July 2004 to Oct. 2005, (b) the two low *z* sites from May–Oct. 2005 (daily rainfall shown near bottom of graph), and (c) the two low *z* sites from Aug. 9–23, 2005. The high *z* site is on a ridge near Echo Lake, ~1.5 km west from the two valley low *z* sites (Fig. 1).

sites spanned an intermediate range of *Tss*; some were warmer than *Ta{z}* and some cooler. Fig. 5b shows (*Tss-Ta{z}*) were smaller for July than for Aug. at most sites, particularly shaded sites, indicating that shading results in larger reduction of *Tss* below *Ta* when solar flux is more intense (July). The smaller July (*Tss-Ta{z}*) also is consistent with smaller *Tss/Tgs* during July than during Aug. (Section 5.2), and more net conductive heat flow downward from shallow soil to depth during July than during Aug. (Supplement 2C).

Fig. 6a, b show no apparent *z* lapse of summer *Tss* among exposed sites, however among forested sites summer *Tss* lapse was about the same as *Ta* lapse. This suggests that at exposed sites the effect on summer *Tss* of *Ta* lapse was largely offset by increase in summer solar radiation flux with increasing *z* (see Section 4.4.1).

3.3. Annual means

For WY 2005, *Tss{an}* ranged from 3.86 °C to 11.33 °C (Table 2) among 82 of the 83 monitored sites (one outlier). *Tss{an}* ranged from (*Ta{an}* − 0.48 °C) to (*Ta{an}* + 5.44 °C) (using L_a = 4.9 °C/km), excluding 2 outliers (Fig. 6c). There were only a few sites for which *Tss{an}* < *Ta{an}* (Fig. 6c), in contrast with summer monthly *Tss* data (Fig. 5b). Offsets of *Tss{an}* above *Ta{an}* may in part be due to seasonal snow-cover insulation (Section 4.4.2).

In contrast with results for summer (Section 3.2), *z* lapse appears to account for a significant fraction of the inter-site variability in *Tss{an}* within each of the major vegetative cover classes (Fig. 6c). At exposed sites, the significant *z* lapse of *Tss{an}*, as contrasted with the apparent absence of significant *Tss* lapse during summer (and winter), may be in part attributable to deeper snow-pack at higher *z*, entailing a longer spring melt period (e.g., Fig. 3a) when *Tss* < *Ta* and snow shields otherwise exposed ground from sunlight. However, the density of vegetative cover (not *z*) is the dominant control on *Tss{an}* inter-site variability within the 0.41 km elevation range of the study sites. Figs. 3–6 show that exposed soils were generally warmest and forested soils coolest, for both summer and mean annual periods.

Fig. 7a shows that warmer *Tss{an}* is associated with warmer Tss_{max}. A nonlinear least-squares fit *Tss{an}* = 1.57 °C + 0.329*Tss{sum}* − 0.393[*Δz*Tss{sum}*] + 3.61*Δz* (where *Tss{sum}* = *[Tss{July}* + *Tss{Aug.}]/2* and *Δz* units are km) fits WY 2005 data from 81 of 83 sites with available data (excluding two 'Echo slide' outliers) very closely (R^2 = 0.833 and std. error = 0.57 °C), demonstrating that *Tss{sum}* and *z* are chief determinants of *Tss{an}*.

3.4. Inter-seasonal ranges and amplitudes

During 2005, (*Ta{July}* – *Ta {Jan.}*) = 21.0 °C, whereas (*Tss{July}*-*Tss{Jan.}*) ranged from 28 °C at an exposed site to 10 °C at a forest site. Fig. 4b shows summer Tss_{max} and winter/spring Tss_{min} are weakly negatively correlated for each vegetation class; well-exposed sites are much warmer in summer and tend to be slightly cooler in winter than forested sites.

Fig. 7a illustrates there is little or no trend in Tss_{min} or Tss_{max} with *z* across the 0.41 km *z* range of sites. For WY 2005, (Tss_{max} - Tss_{min}) ranged among low *z* sites from 30.6 °C at an exposed site to 12.2 °C at a forest site, and among high *z* sites from 30.0 °C at an exposed site to 11.1 °C at a forest site; by comparison ($Ta_{max} - Ta_{min}$) = 32.1 °C. Winter *Ta* amplitude (*Ta{an}* - Ta_{min}) = 16.6 °C is much larger than winter *Tss* amplitude $A_w \equiv$ (*Tss{an}* – Tss_{min}) at each site. Fig. 7a also shows $A_s > A_w$ for all sites, where $A_s \equiv$ (Tss_{max} - *Tss{an}*).

In areas without seasonal snow-cover, annual series of daily mean *Tss* are often well-approximated as a sinusoidal oscillation of period 1 year (see Section 5.2.2). For such a sinusoidal oscillation $A_w/A_s \sim 1$. Fig. 7b illustrates that among the Tahoe sites, A_w/A_s ranged from 0.74 to 0.31, decreasing with increasing *z*. These small values of A_w/A_s are a measure of the departure of the *Tss* time series at each site from a model sinusoidal oscillation, and are attributable to the long duration of seasonal snow-cover (see Fig. 3a). Fig. 7b also shows extrapolations of the least-squares fit trend-line thru the Tahoe data points. Remarkably, the trend-line intersects A_w/A_s = 1 at *z* = 0.8 km: snow-cover observations in the Sierra foothills to the west show there is little or no seasonal snow-cover at *z* < ~0.5 to ~ 1.0 km (Freeman, 2009; Minder and Kingsmill, 2013; Hatchett et al., 2017), suggesting that indeed $A_w/A_s \sim 1$ below *z* ~ 0.8 km. The same trend-line intersects A_w/A_s = 0 at *z* = 3.5 km, which is somewhat higher than the elevation above which

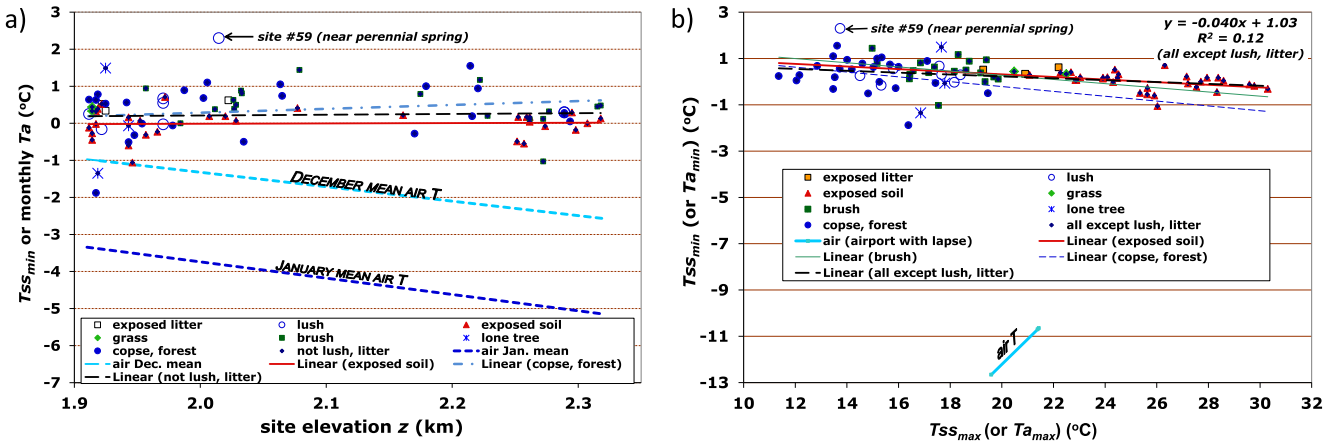

Fig. 4. Tss_{min} for WY 2005 vs. a) site z, and b) Tss_{max}, at each soil site with available data. a) shows there is no trend of Tss_{min} with z, and that Tss_{min} are markedly warmer than Dec. and Jan. mean Ta, especially at high z sites. b) shows that sites with warmer summer Tss_{max} tend to have cooler winter Tss_{min}.

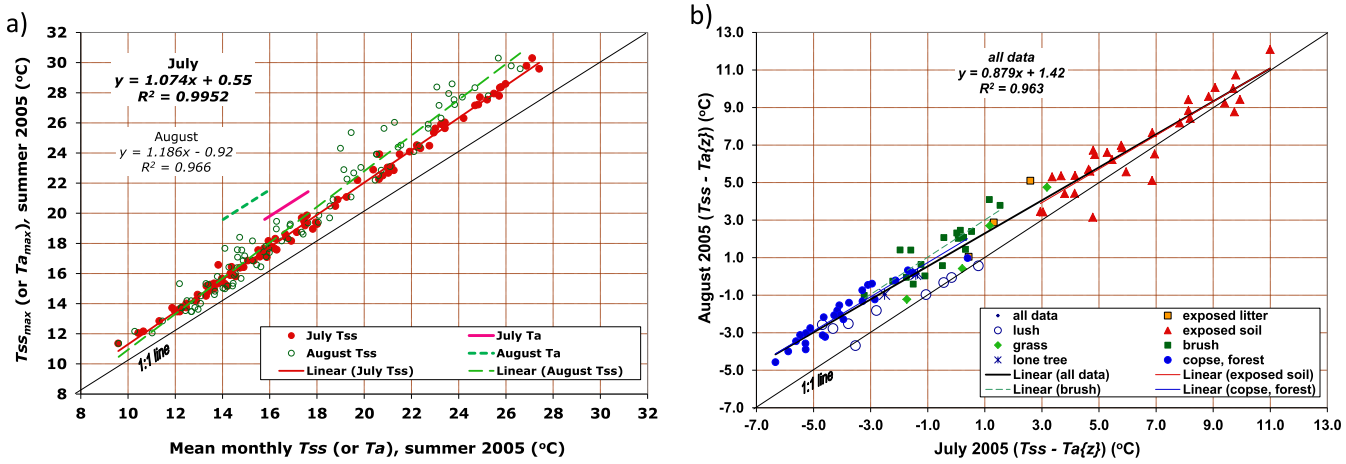

Fig. 5. a) Summer 2005 Tss_{max} vs. $Tss\{July\}$ and $Tss\{Aug.\}$ at each soil site with available data. Ta_{max} vs. monthly $Ta\{z\}$ are also shown for the z range of sites. b) Aug. 2005 mean monthly ($Tss–Ta\{z\}$) vs. July 2005 mean monthly ($Tss–Ta\{z\}$), at each soil site with available data. a) shows Tss_{max} are offset above $Tss\{July\}$ by only ~1 °C to ~3 °C at all sites, and b) shows July ($Tss–Ta$) < Aug. ($Tss–Ta$) at all forested sites.

perennial snow/ice patches (z > ~2.5 km) and small glaciers (z > ~2.8 km) are found near sections of the Tahoe Basin drainage divide west and south from the study area (Raub et al., 2006). The lower bound of the 99% prediction interval (Fig. 7b) intersects $A_w/A_s = 0$ at z ~ 2.8 km, the lower limit of observed glaciation.

3.5. Inter-annual variations

Data were recovered from ten of the twelve probes left in place until fall 2006 or 2007. All ten probes were sited between 1.91 km and 1.94 km elevations. Tss data for these sites are tabulated in Supplement 5, together with multi-annual data for Ta_0 and precipitation.

Among the 8 sites monitored during WY 2007, $Tss\{an\}$ ranged from 6.07 °C to 13.14 °C within a z range of 0.01 km, and ($Ta\{an\}$ − 0.85 °C) ≤ $Tss\{an\}$ ≤ ($Ta\{an\}$ + 6.16 °C). This 7.0 °C inter-site range is larger than the 5.9 °C range of ($Tss\{an\}$ – $Ta\{an\}$) among 81 of the 83 sites monitored during WY 2005 (Section 3.3 above), likely due to WY 2007 being a dry year with early snowmelt and scant summer rainfall. During summers 2004 to 2007, Tss_{max} occurred between mid-July and late Aug. at all sites monitored, and changed by < 2.3 °C between summers. Inter-annual changes in Tss during summer and in $Tss\{an\}$ were largest at exposed sites. Inter-annual changes in Ta and precipitation accounted for a substantial fraction (but not all) of these inter-annual changes in observed Tss (see Supplement 5B).

During most of each seasonal snow-cover period of WYs 2005, 2006, and 2007, Tss was near 0 °C at all sites monitored. During these three cold seasons there was only one episode of widespread ground freezing. This episode started in mid-Jan. 2007 after a warm period of snowmelt; during subsequent Ta cooling, daily mean Tss dropped below 0 °C at all ten sites and below −2°C at three of these sites (Tss_{min} were −2.2 °C, −4.7 °C, and −5.5 °C, with Tss < -2°C for durations of 1, 12, and 12 days, respectively). Snow-cover resumed late Jan. to early Feb. and Tss recovered to above 0 °C at all sites well before spring melt.

4. Results 2: Model fits to soil temperature data, and model application and evaluation

4.1. Model fits to summer monthly mean Tss data

Data for mean monthly Tss for July and August 2005 from 83 of 95 sites are regressed against model form Eq. (9), yielding least-squares estimates of the coefficients $C1'$, C_{LO}, C_h' for July 2005 and for August 2005 (Table 3). The calibrated model equations are:

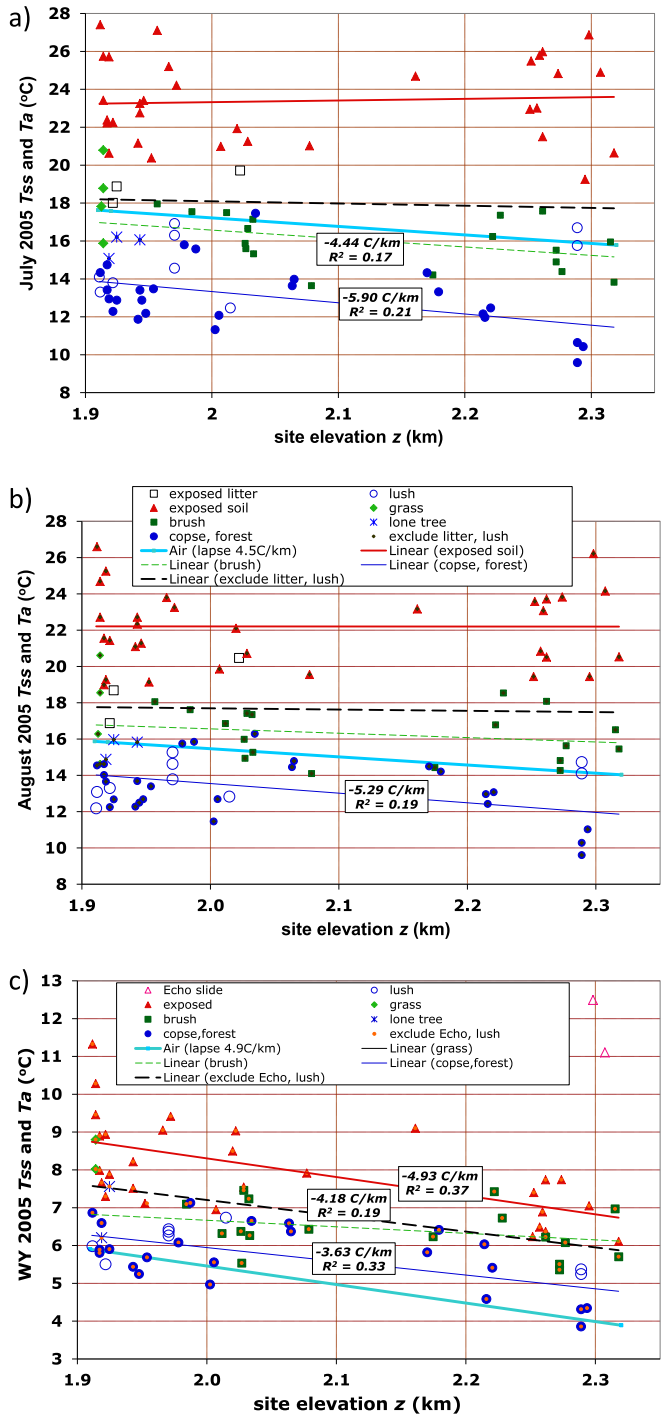

Fig. 6. *Ta{z}* and *Tss* data vs. *z* at each soil site with data available for a) July 2005 b) Aug. 2005, and c) WY 2005. The legend in b) is also for a). Linear least-squares fit equations are shown (boxes intersecting fit lines) for vegetation classes with $R^2 > 0.1$. The graphs show that across warm (exposed) sites there is no apparent *z* lapse of monthly mean *Tss* during summer.

$$Tss\{July\} = Ta\{z\} + 2.78\Delta z + [-2.40 - LE' + 53.5(1-\alpha)(1-f)\cdot Rn_O\{r\}\cdot \exp(0.0953\Delta z) + \varepsilon_g(\varepsilon_{sv}-1)(Ta\{z\})^4/(4Ta_O^3)] /[1.20(1-0.44f) + \varepsilon_g(Ta\{z\}/Ta_O)^3] \quad (11)$$

$$Tss\{Aug.\} = Ta\{z\} + 2.53\Delta z + [(+1.44 - LE' + 50.6(1-\alpha)(1-f)\cdot Rn_O\{r\}\exp(0.0953\Delta z) + \varepsilon_g(\varepsilon_{sv}-1)(Ta\{z\})^4/(4Ta_O^3)] /[1.09(1-0.44f) + \varepsilon_g(Ta\{z\}/Ta_O)^3] \quad (12)$$

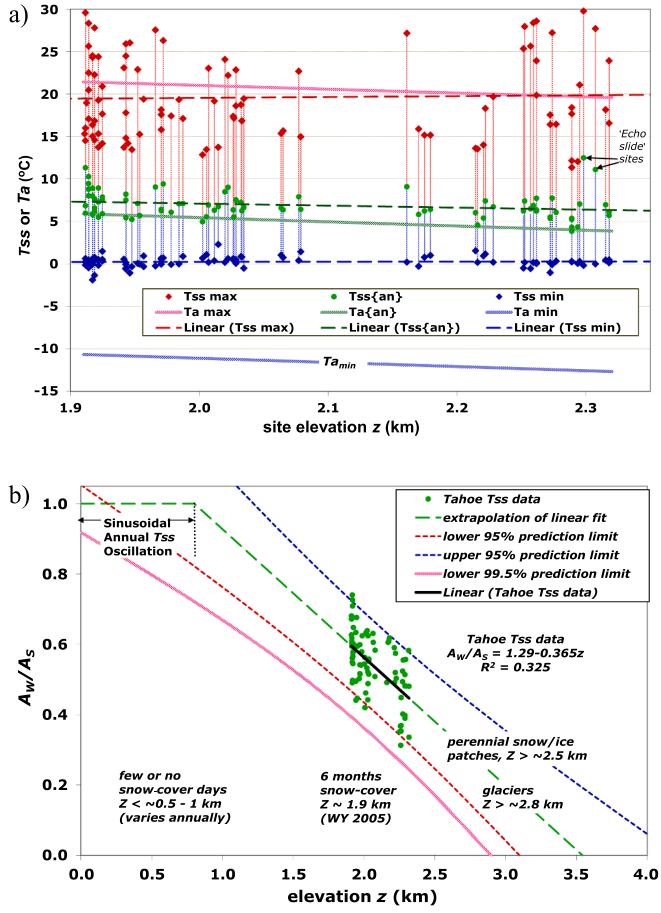

Fig. 7. a) Maximum, mean, and minimum 24-hr mean *Tss* and *Ta* values during WY 2005 at each Tahoe soil site. b) $A_w/A_s = [(Tss\{an\}-Tss_{min})/(Tss_{max}-Tss\{an\})]$ vs. *z* at each Tahoe soil site with annual data (except two 'Echo slide' outliers). The linear least squares fit to the Tahoe data in b) is extrapolated to higher and lower *z*. Observed durations of northern Sierra seasonal snow (or ice) cover at several *z* are described near bottom of graph b).

Table 3
Fitted coefficient values for summer and annual soil *T* models.

	Unit	July 2005 (83 sites[a])	August 2005 (83 sites[a])	WY 2005 (73 sites[b])
C_{LO}	°C/km	+2.78 ± 2.64 (p = 0.085)	+2.53 ± 2.35 (p = 0.077)	+1.09 ± 0.91[c] (p = 0.049)
C1′	°C	−2.40 ± 0.97 (p = 0.0001)	+1.44 ± 0.86 (p = 0.0063)	NA –
C_h'	–	+1.20 ± 0.20 (p < 0.00001)	+1.09 ± 0.18 (p < 0.00001)	+3.28 ± 0.58 (p < 0.00001)
C0	°C	NA –	NA –	+2.60 ± 0.19 (p < 0.00001)
C_{Lr}	1/km	NA –	NA –	−0.80 ± 0.75[c] (p = 0.081)

Coefficient values determined by least-squares regression.
Least-squares values with +/− for 90% confidence limits. p = probability that value of coefficient is zero or of opposite sign.
[a] fit for sites with summer 2005 *Tss* data (except lush and exposed litter).
[b] fit for sites with WY 2005 *Tss* data (except lush & Echo slide).
[c] regressed values of C_{Lr} and C_{LO} are highly negatively correlated.

where $Ta\{z\} = Ta_O - 6.0\Delta z$. For July 2005, Ta_o = 17.6°C = 290.7°K and $\varepsilon_{sv} \approx 0.94(1-F_{sky}) + F_{sky}[0.55{\cdot}f{\cdot}0.96 + 0.7619(1-0.55f)]$. For Aug. 2005, Ta_o = 15.8 °C = 289.0 °K and $\varepsilon_{sv} \approx 0.94(1-F_{sky}) + F_{sky}[0.55{\cdot}f{\cdot}0.96 + 0.7616(1-0.55f)]$. Model *Tss{July}* and *Tss{Aug.}* values computed for each site using Eqs. (11), (12) are listed in

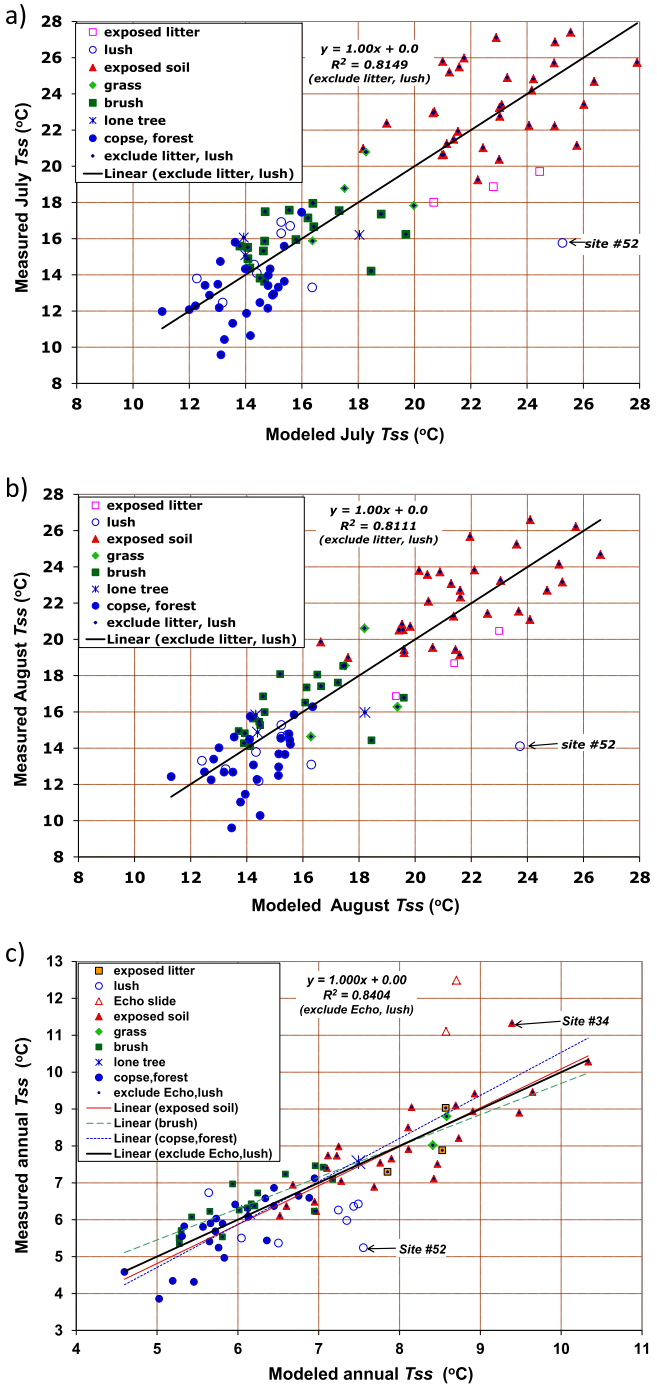

Fig. 8. *Tss* data vs. model computed *Tss* values (from Eqs. (11), (12), or (13)) for each soil site with available data for a) July 2005 (95 sites), b) Aug. 2005 (95 sites), and c) WY 2005 (83 sites). The thick line in each graph is the least-squares linear fit to all sites except those depicted with hollow symbols.

Table S1–3 of Supplement 1. Fig. 8a, b illustrate that for July and for Aug., a single regression line spans all the vegetative cover classes, from fully exposed (non-vegetated) to densely forested. 81% of the inter-site variance in the *Tss* data (and in (*Tss* – *Ta{z}*)) is accounted for by model Eqs. (11), (12).

12 sites are not included in regressions for July and Aug. *Tss*, including 9 'lush' sites observed to have wet topsoil thru late summer (sites near springs, ponds or wetland areas with very shallow water table), and 3 exposed soil sites with a thick (~2 cm) cover of litter (leafs, pine needles, twigs, bark etc.). Such sites could be negative outliers, since the cooling effects of consistently wet summer topsoil and shielding/insulating effects of thick litter cover are not accounted for in the surface *T* model. *Tss* data for all exposed litter sites are below the regression line during July and Aug. (Fig. 8a, b). During Aug., *Tss* data are at or below the regression line at all but one of the lush sites (Fig. 8b).

4.2. Model fit to annual mean Tss data

Data for mean annual *Tss* for WY 2005 from 73 of 83 sites are regressed against model form Eq. (10); yielding least-squares estimates of the coefficients *C0*, C_{LO}, C_{Lr}, C_h' for WY 2005 (Table 3). The resulting calibrated model equation for *Tss{an}* is

$$\begin{aligned} Tss\{an\} = Ta\{z\} + 1.09\Delta z + 2.60 + [\exp(-0.801\Delta z)]\cdot \\ [LE' + 41.0(1-\alpha)(1-f)\cdot Rn_O\{r\}\cdot\exp(0.0953\Delta z) \\ + \varepsilon_g(\varepsilon_{sv}-1)(Ta\{z\})^4/(4Ta_O^3)] \\ /[3.28(1-0.44f) + \varepsilon_g(Ta\{z\}/Ta_O)^3] \end{aligned} \quad (13)$$

where $Ta\{z\} = Ta_O - 6.0\Delta z$. For WY 2005, Ta_O = 5.85°C = 279.0°K and $\varepsilon_{sv} \approx 0.948(1 - F_{sky}) + F_{sky}[0.55{\cdot}f{\cdot}0.96 + 0.7413(1 - 0.55f)]$. Model *Tss{an}* values computed for each site using Eq. (13) are listed in Table S1–3 of Supplement 1. Fig. 8c shows a single regression line fits tightly (R^2 = 0.84) across all classes of vegetation.

Eight 'lush' sites with damp topsoil thru late summer are not included in the *Tss{an}* regression. *Tss{an}* at the lush sites are below the regression line (Fig. 8c), with the exception of one site near a perennial spring, which was the warmest of all sites during winter (Fig. 4a, b). Two sites in steep granitic bedrock slabs, where snowpack slid off during warm spells in winter ('Echo slide' sites), were also eliminated from the regression (positive outliers, Fig. 8c). One exposed site (#34) may also be a positive outlier for annual (Fig. 8c) but not summer averaging periods; this site is among the easternmost sites (Fig. 1) in the study area and has earlier snowmelt than other sites, likely due to less snowfall at this easterly location. The three exposed sites with thick (>2 cm) litter cover are included in the annual regression model (Fig. 8c); the soil insulation imparted by litter cover is expected to attenuate the amplitude of the *Tss* seasonal oscillation, but not to affect *Tss{an}* (e.g., Paul et al., 2004).

Of the 24 sites for which Tss_{min} < 0 °C during WY 2005 (Section 3.1), 18 had data logged for the entire WY 2005 and were neither 'lush' nor 'Echo slide' sites. *Tss{an}* data for these 18 sites are centered about the 1:1 line in Fig. 8c; the median and mean values of the difference between data and model values of *Tss{an}* for these sites are −0.04 °C and +0.05 °C, respectively. This indicates that model Eq. (10) is comparably accurate for sites which have a brief episode of shallow soil freeze during winter as for sites that do not freeze.

4.3. Resolving the effects of spatial variations of soil site parameters on Tss

Data and model results in Sections 3, 4.1 and 4.2 above show that warmer *Tss* is associated with dryer soils, lower elevation, and less vegetative cover, along with other factors. Here, the influence of the range of estimated values (among all monitored soil sites) of each of four parameters (i) soil evaporation *E*, (ii) elevation *z*, (iii) site orientation *r* (i.e., *S* and aspect) and (iv) shading *f* on the range of *Tss* in the Tahoe study area are each quantitatively evaluated using the calibrated *Tss* model Eqs. (11), (12), and (13).

Fig. 9 displays inter-site ranges of model *Tss* values computed (using Eqs. (11) to (13)) when one model parameter is varied across it's range of estimated values among all sites (Table 1, Fig. 2a, b) while all other parameters are fixed at their site-mean values (Table 1). When *E* varies across its range while all other site-dependent parameters (*z*, *r*, *f*, α, ε_g, ε_{sv}) are fixed at their site-mean values, resultant widths of inter-site ranges of model *Tss* values are narrow; specifically only 1.1 °C for July, 1.4 °C for Aug. and 0.8 °C for the water-year. Even narrower ranges of

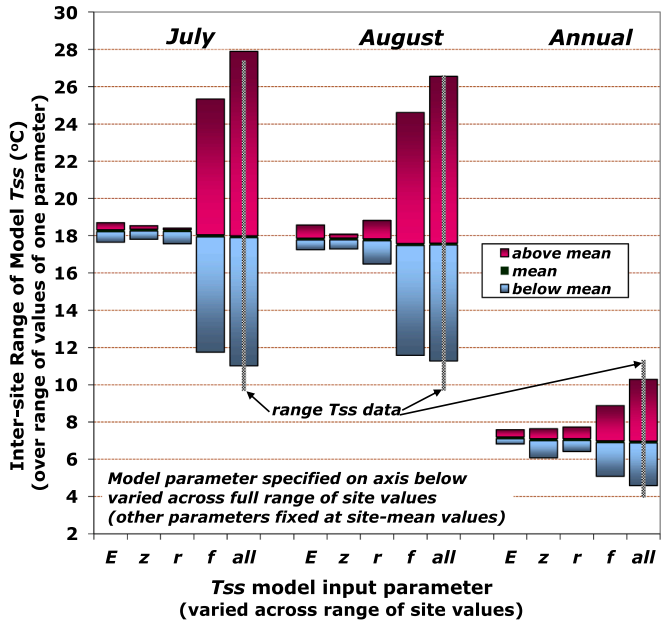

Fig. 9. Each bar spans the inter-site range of model computed *Tss* (July, Aug., or annual mean) among all the Tahoe soil sites (95 for summer 2005, 83 for WY 2005) under the conditions specified in the graph (see also Section 4.3). The "all" category denotes the condition where every parameter takes on its estimated site value at each site. The thick vertical line in the middle of each 'all' category bar spans the range of *Tss* data among all soil sites (note: outlier annual data point for one 'Echo slide' site is excluded).

Tss result for July and Aug. when only z is varied. By contrast, when f (and only f) varies across its range, resultant ranges of model *Tss* for summer monthly and annual periods are nearly as wide as when all parameters vary across their ranges.

Fig. 10 displays inter-site ranges of model *Tss* values computed (using Eqs. (11) to (13)) when estimated values of all parameters are varied across their ranges among all sites, except for one parameter whose value is fixed at either it's minimum, mean, or maximum value among all sites (Table 1). Fig. 10 illustrates that when E is fixed at one value, resultant inter-site ranges of model *Tss* values are broad; nearly as wide as when E is not fixed and together with all other parameters varies across its full range of values. Similar wide ranges of *Tss* result when z is the fixed parameter: at z = 1.91(2.32) km, the width of the inter-site range of model *Tss* is 16.1 °C (16.9 °C) for July, 14.4 °C (15.2 °C) for Aug., and 5.65 °C (4.27 °C) for WY 2005. By contrast, when f (and only f) is fixed at one value, resultant inter-site ranges of *Tss* are narrow; specifically for both July and Aug., inter-site ranges of model *Tss* for f fixed at minimum, mean, or maximum values do not overlap (Fig. 10). Note changes in r appreciably affect the maximum value of *Tss* for each time period but not the minimum, since f controls the fraction of over-canopy insolation $Rc\{r,z\}$ that reaches ground surface.

Figs. 9 and 10 are complementary, together indicating that spatial variations of E, z and r (and also of the remaining site-dependent parameters α, ε_g, and ε_{sv}, not shown in the figures) have only a small to moderate influence on the spatial variations of *Tss* in the Tahoe study area, whereas spatial variations of f exert a dominant influence. A possible exception is a lush site that was anomalously non-vegetated, at which E was likely substantially larger than the maximum E used for Figs. 9 and 10 (see Section 4.4.4). Vegetation density affects nearly every term in the surface energy balance Eq. (1) and in Eqs. (9) thru (13) for *Tss*, either directly thru f or indirectly, as described in Supplement 2A.

4.4. Additional analyses and evaluation of model results

4.4.1. Elevation lapses

The calibrated value of the z lapse coefficient C_{LO} for any period (July, Aug., or annual) helps to compensate for a combination of the

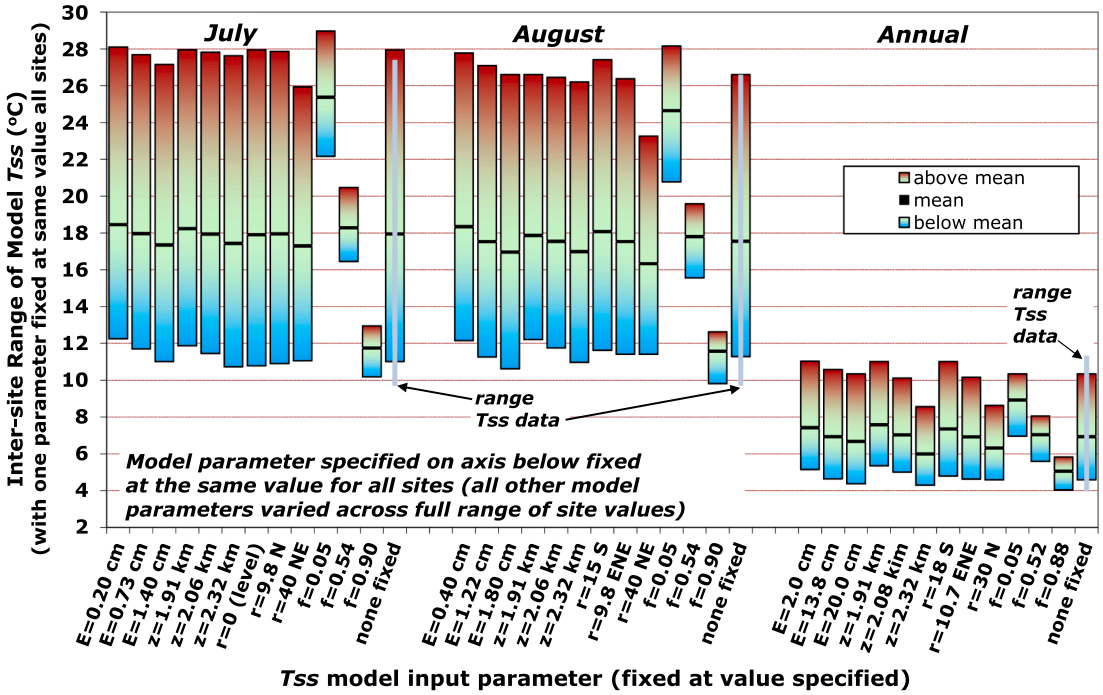

Fig. 10. Each bar spans the inter-site range of model computed *Tss* (July, Aug., or annual mean) among all the Tahoe soil sites (95 for summer 2005, 83 for WY 2005) under the conditions specified in the graph (see also Section 4.3). For r, the axis is labeled with the values of slope (degrees) and aspect (N = north, E = east, S = south) corresponding to the maximum, mean, and minimum values of $Rn_o\{r\}$ (see Table 1). The "none fixed" category denotes the condition where every parameter takes on its estimated site value at each site (same as 'all' category in Fig. 9). The thick vertical line in the middle of each 'none fixed' category bar spans the range of *Tss* data among all soil sites (as in Fig. 9).

following: (i) error in the estimate of the *Ta* lapse factor L_a for that period (ii) error in the estimate of the insolation lapse factor L_R for that period, (iii) for annual periods, lapse in effects of snow-cover on *Tss{an}* that are not addressed by C_{Lr}, and (iv) presence of lapses in other energy balance terms (e.g., latent and sensible heat) which are not formulated in Section 2 model equations. Model calibrated values of (L_a - C_{LO}) (see Eqs. (9), (10)) are 4.91 °C/km, 3.22 °C/km, and 3.47 °C/km (Tables 1 and 3) for WY 2005, July 2005, and Aug. 2005, respectively; slightly smaller than the wet air adiabatic lapses at 800 mbar (atmospheric pressure at $z \sim 2.0$ km) and mean *Ta* for these time periods. Analyses (see Supplement 3E) using these calibrated (L_a - C_{LO}) values together with other published estimates of *Ta* lapse in the Tahoe Basin indicate:

(a) For WY 2005, an estimate of annual mean $L_a \sim 4.9$ +/- 0.5 °C/km is more reliable than the initial L_a estimate in Table 1, but the annual mean L_R estimate in Table 1 is supported.
(b) For both July 2005 and Aug. 2005, an estimate of monthly mean $L_a \sim 4.5$ +/- 1.1 °C/km is more reliable than the initial L_a estimate in Table 1, and the summer L_R value in Table 1 may significantly underestimate actual L_R during summer 2005.
(c) C_{Lr} accounts for most of the *z*-dependent effects of snow-cover on *Tss{an}*. From Eqs. (10) and (13), this entails that for the warmest (i.e., exposed) sites, as seasonal snow-cover duration decreases along with decreasing *z*, then (*Tss{an}* – *Ta{an}*) increases; however at the coolest (i.e., densely forested, *Tss{an}* < *Ta{an}*) sites (*Tss{an}* – *Ta{an}*) decreases.

The least-squares calibrated value of the lapse coefficient C_{Lr} is −0.80/km (Table 3), corresponding to a reduction in inter-site range of annual (*Tss* – *Ta{z}*) of ~ 28% up the 0.41 km *z* range of study sites (see also Fig. 6c). Similarly, the observed *z* lapse of days without snow-cover during WY 2005 decreased up the 0.41 km *z* range of study sites from ~ 26 weeks to ~ 20 weeks; i.e., a ~ 23% decrease in days without snow-cover. This suggests the C_{Lr} term accounts for the effect on *Tss{an}* of the *z* lapse of seasonal snow-cover duration.

4.4.2. Calibration coefficients C_h', *C1′*, *C0* and effects of input bias

C_h' is associated with convection (Section 2.3.1). For summer averaging periods, C_h' in Eq. (9) also incorporates part of (as does *C1′*) conductive heat flow downward from the soil surface and associated attenuation of *Tss* relative to *Tgs* (Sections 2.3, 5.2.1). Conductive heat flow and *Tss* attenuation are each more pronounced during July than Aug. (Supplement 2B, C), consistent with the smaller value of *C1′* and the larger value of C_h' in July as compared with Aug. (Table 3). The fitted C_h' value for the annual period is much larger (as compared to July and Aug., Table 3), since annual C_h' incorporates most of the attenuation of inter-site differences in *Tss{an}*. This attenuation occurs due to the long period of seasonal snow-cover, when all sites have observed seasonal mean *Tss* values within a common narrow range near 0 °C (note from Eq. (10) that larger C_h' entails smaller inter-site range of *Tss{an}*).

The value of *C0* (Table 3) is not a measure of the site-mean amount of *Tss{an}* warming provided by snow-cover insulation, since *C0* also incorporates the effect of use of α_{snow} and ε_{snow} in determination of annual mean values of α and ε_g (Supplement 1C) that are input to Eq. (10). Seasonal snow-cover often but not always results in *Tss{an}* warming, depending on the times of onset and melt of the snow-cover (Zhang, 2005).

Each of the *Ci* also incorporates some of the systematic errors in inputs to the model regression equation from which it was calibrated. There is large uncertainty (thus possible substantial bias) in summer and annual estimates of Rc_o (Table 1) and of *E* (Fig. 2b), which were input to model Eqs. (9) and (10) for *Tss* calibration. Possible bias in Rc_o and *E* estimates and in parameter estimates (notably for mean annual albedo) may have significantly affected values of the fitted coefficients *Ci* listed in Table 3 for summer and annual periods (see Supplement 1D). Other types of systematic errors can also influence the *Ci* (Section 5.2.1).

Table 4
Statistics of calibration fits of soil *T* models.

Statistical parameter	unit	July 2005	Aug. 2005	WY 2005
n	–	83	83	73
p	–	3	3	4
R^2	–	0.8149	0.8111	0.8404
Mean *e*	°C	0.00	0.00	0.00
Mean |*e*|	°C	1.67	1.53	0.47
s_e	°C	2.088	1.846	0.565
RMSE	°C	2.113	1.869	0.577
Skew *e*	–	0.06	−0.25	0.07
Excess kurtosis *e*	–	−0.42	−0.53	1.04
s_d	°C	4.852	4.247	1.414
s_m	°C	4.384	3.831	1.296
s_d/*RMSE*	–	2.30	2.27	2.45
Rge{Tss$_d$}	°C	17.82	17.00	7.47
Rge{Tss$_m$}	°C	16.88	15.30	5.74
Rge{Tss$_d$}/2RMSE	–	4.22	4.55	6.48

n = # soil monitoring sites used for model calibration.
p = # calibration coefficients in *Tss* model.
R^2 = coefficient of multiple determination.
e = residual error = Tss_d–Tss_m.
Tss_d = data value *Tss*, Tss_m = model value *Tss*.
s_e, s_d, s_m = std. dev. of *e*, Tss_d, Tss_m.
Mean |*e*| = $[\Sigma|e|]/(n\text{-}p)$.
RMSE = root mean square *e* = $[\Sigma(e)^2/(n\text{-}p)]^{0.5}$.
Rge{$Tss_{d(m)}$} = range of $Tss_{d(m)}$ (i.e. max.–min.)

4.4.3. Model fidelity

The standard deviations s_e of *Tss* data deviations from the least-squares model regression lines are 2.09, 1.85, and 0.56 °C for July, Aug., and WY 2005, respectively; small relative to inter-site ranges of *Tss* data (Table 4 and Fig. 8a, b, c). Temperature sensor measurement errors, including drift (<0.15 °C/yr) do not contribute significantly to scatter of *Tss* data about the model regression fits. Discrepancies between the *Tss* data and models (i.e., scatter about the least-squares regression lines) are attributable to:

(I) Errors in the estimated values of site-specific terms and parameters *Ta{z}*, *Rc{r,z}*, *f*, *E*, α, ε_g, ε_{sv} that are used in the *Tss* models. Site-specific errors in estimates of shading *f* and soil *E* (*LE*) likely constitute most of the site parameter estimate error contribution to the regression model scatter, for both summer and annual time periods.
(II) Errors from (i) simplifications in formulations of energy balance terms (Section 2.3.1) used in model Eqs. (9), (10), notably for sensible heat exchange and snow-cover effects (ii) use of time-average parameter and data values in Eqs. (9), (10), and (iii) (for summer) small inter-site variations in (*Tss* - *Tgs*) and *Tss/Tgs* (°C/°C) (Section 5.2.1 and Supplement 2B).

Error sources (I) and (II) above are judged to each contribute comparably to the scatter of data about the regression model fits for July, August, and annual *Tss*. Model fit to data could be improved significantly (to $R^2 > \sim 0.90$) by using highly accurate estimates of site-specific parameters; however such improvement is likely limited to $R^2 < \sim 0.95$ due to (II).

4.4.4. Soil evaporation at perennially wet sites

The estimates of *E* used in model Eqs. (11), (12), (13) for perennially damp ('lush') sites (Supplement 1C) are the same values used for non-lush sites with that vegetation (i.e., grass, except at site #52). For lush sites, the negative offsets of *Tss* data from the regression model fits for Aug. and annual periods (Fig. 8b, c) are likely due to the model input *E* values moderately underestimating actual *E*, and possibly to

transpirative cooling (Supplement 4A).

One of the 'lush' sites (#52) is a non-vegetated site of damp exposed soil ($f \sim 0.15$); *Tss* data for this site are clear negative outliers from the regression model fits (Fig. 8a, b, c). Supplement 4B details several conventional direct estimates of *E* for wet topsoil with site #52 exposure conditions for July 2005, Aug. 2005, and WY 2005. These estimates of *E* are many-fold larger than those used as input for site #52 model *Tss*, and fully account for the large offsets of model *Tss* values for site #52 below the regression lines in Fig. 8a, b, c.

4.5. Model Tss performance for additional years

We were not able to obtain adequate meteorology data for WY 2006 and 2007 to compute model *Tss* output for these years using Eqs. (9), (10) and WY 2005 calibrated *Ci* values (Table 3). Preliminary analyses indicate that model *Tss{July}* and *Tss{Aug.}* estimates are comparably accurate across summers 2005 to 2007. This entails that model Eq. (9) with summer *Ci* values from Table 3 (with C_h adjusted for wind speed; see Supplement 2E) are accurate for all summers, not just summer 2005. Inter-annual changes in bias of model input values (notably for Rc_0, *LE*) could affect the accuracy of model output *Tss* values.

Preliminary model *Tss{an}* estimates for WY 2006 and particularly 2007 (a dry year with early snowmelt) are not as accurate as for WY 2005. WY 2005 annual *Ci* values in Table 3 were likely influenced by WY 2005 snow-cover characteristics, such as onset date, melt completion date, and total days of snow-cover, consistent with results of physical models parameterized for input of seasonal snow coverage details (e.g., Goodrich, 1982) and with field observations (Zhang, 2005). Use of Eq. (10) for *Tss{an}* with Table 3 *Ci* values may be highly accurate only for years with above average snowfall and similar snow-cover dates and durations as WY 2005 (see also Section 3.1). For other years with light snowfall and much shorter snow-cover duration, the annual *Ci* values may need to be re-calibrated.

5. Discussion

5.1. Comparisons of soil T observations at Tahoe with other areas

At Tahoe, both the warmest and coldest Tss_{min} sites (Section 3.1) had plant cover, as has been observed elsewhere (e.g., Brearshears et al., 1998). The thawing of frozen ground under snow-cover observed during winters at Tahoe (Sections 3.1, 3.5) has also been reported elsewhere (Zhang, 2005), and indicates that the amount of seasonally stored heat conducted upward from depth during winter is sufficient to thaw shallow soil that freezes as late as mid-January in the Tahoe study area. These and other *Tss* patterns during winter (Sections 3.1, 3.5) are consistent with those reported by Maurer and Bowling (2014) for interior western U.S. mountains, attributable to the insulation provided by deep winter snow-cover.

Inter-site ranges of summer monthly mean *Tss* of 17.8 °C (July) and 17.0 °C (Aug.) at Tahoe (Section 3.2) each occurred within a *z* range of 0.02 km, and are about twice as wide as the range in summer monthly mean *Ts* reported for a montane area in Canada (Ballard, 1972). Supplement 2B model results for *Tgs* (using *Tss* input data) indicate that during sunny summer days, well-exposed sites at Tahoe have diurnal ranges of *Tgs* exceeding 40 °C; also intra-daily peaks of *Tgs* at well exposed sites are >25 °C warmer than intra-daily peaks of *Tgs* at dense forest sites, which is broader than an inter-site range in summer mid-day land surface *T* of 18 °C observed in the White Mountains (Graham et al., 2012). In the Tahoe region, vegetation density, local slope and aspect, soil moisture, and other factors that govern *Ts* vary across multiple spatial scales. It follows that *Ts* also varies across multiple spatial scales, in accord with conclusions of Wundram et al. (2010) for mountain areas.

The inter-site ranges of (*Tss{an}-Ta{an}*) observed at Tahoe (Section 3.5) are about twice as wide as those for *Ts{an}* reported in other areas (e.g., Chapman et al., 1992; Taniguchi et al., 1999; Jimenez et al., 2007; see also Introduction), approaching the 9 °C range (*Ta{an}*-2°C < *Ts{an}* < *Ta{an}* + 7 °C) estimated across Canada (Zhang et al., 2005). Site-mean (*Tss{an}-Ta{an}*) for the 83 Tahoe sites was +1.84 °C for WY 2005, slightly below the areal mean estimate for (*Ts{an}-Ta{an}*) of +2.5 °C for Canada (Zhang et al., 2005).

5.2. Soil T model assessment and applicability

5.2.1. Errors inherent to formulation and use of the temperature models

Simplifications in formulation of the surface energy balance terms (Section 2), notably for sensible heat exchange for both snow-free and annual periods, heat conduction for snow-free periods (incorporated into Eq. (9) *Ci*), and the effects of snow-cover for annual periods (incorporated into Eq. (10) *Ci*), may limit the potential accuracy of model Eqs. (9) and (10). Supplement 2A discusses these and other simplifications in model formulation.

The regression models Eqs. (9), (10) are based on instantaneous values for energy flux parameters and terms, most of which vary on sub-daily (e.g., diurnal), inter-daily, and seasonal time scales. However, time-averaged (monthly or annual) values of *Ta*, radiation, soil *E*, and other terms and parameters were used as input to the models (note wind speed is incorporated into the calibration coefficient C_h, such that C_h also varies on all time scales). In general there may be discrepancies in model *Tgs* results between: (i) the use of time-averaged values of parameters and terms in the quotient on the right-hand side of Eqs. (9), (10), and (ii) the time average of instantaneous values of this quotient.

As discussed in Section 2.3.2, Eq. (9) is derived for *Tgs*, yet is used in this manuscript to model *Tss*. It is expected that 24-hr (and multi-day) mean *Tss* is typically slightly cooler than overlying 24-hr mean *Tgs* during summer. Specifically, for the Tahoe study sites at 15 cm depth, Supplement 2B shows that *Tss{July}* values (°C) are between ~3% to ~10% smaller than *Tgs{July}* values (°C), and *Tss{Aug.}* values (°C) are between ~1.5% to ~5.5% smaller than *Tgs{Aug.}* values (°C). Site-mean attenuation of *Tss*(°C) below *Tgs*(°C) for the Tahoe soil sites (~6% for July and ~ 3.5% for Aug.) is incorporated into calibrated values of *C1′* and C_h'. Inter-site variations in κ and in summer amplitude of the annual *Tss* oscillation cause inter-site variations in the amount of this summer *Tss* attenuation (Supplement 2B), which contribute to data scatter about July and Aug. model best-fit lines (Section 4.4.3).

The impact on model *Tss* of the errors inherent in model formulation and use discussed above, as well as possible bias in our model input and parameter values (Section 4.4.2), are largely (but not completely) offset by the calibrated *Ci* values, as shown by the close agreement (high R^2) between observed and modeled *Tss* (Section 4.4.3).

5.2.2. Review of soil T model suitability for areas with diverse ground surface environments and seasonal snow-cover

Many investigators have used a sinusoidal waveform model for *Tss* of period 1 year to approximate seasonal *Tss* changes (e.g., Lin, 1980; Krarti et al., 1995; Mihalakakou et al., 1997; Paul et al., 2004; Badache et al., 2016). However, a sinusoidal waveform may not well-approximate temporal *Tss* profiles in areas with long duration seasonal snow-cover (e.g., Section 3.4, Figs. 3a, 7b). Empirical models have been used successfully for *Tss* (e.g., Paul et al., 2004), however physics-based models can be more reliably applied to a wide variety of site environments and regions, and enable improvement of model performance thru refinements in model parameterization and more accurate input values. Many *Tss* models parameterize the physics of the ground surface energy balance (e.g., Lin, 1980; Krarti et al., 1995; Mihalakakou et al., 1997; Badache et al., 2016), but are not formulated for vegetative cover. Others (e.g., Deardorff, 1978; Herb et al., 2008) have coupled a canopy energy balance to the ground surface energy balance. Such coupling contributes substantially to modeling complexity, and it is not clear how significant the gain in accuracy is of model *Tss* output.

Many physics-based *Tss* models are not calibrated (e.g., Deardorff,

1978; Lin, 1980; Krarti et al., 1995; Mihalakakou et al., 1997). Large uncertainty in the convection term alone (e.g., Ouzzane et al., 2014; Badache et al., 2016), together with significant uncertainties typically associated with soil properties and moisture state, vegetative cover properties, and meteorology and solar radiation data strongly suggest that calibration can enable more reliably accurate model *Tss* output. Some models calibrate over time separately at each of several sites; resultant calibration factor values differ between sites (e.g. Herb et al., 2008). Following Paul et al. (2004), in this article 'regional' calibrated *Ci* each have a fixed value common to all locations in the study area. To our knowledge, the *Tss* models in this article are the only energy balance based models that combine: (i) a parameter for vegetation and terrain shading (without coupling a foliage energy balance), (ii) regional calibration coefficients *Ci*, and (iii) for annual periods, applicability to areas with long duration seasonal snow-cover (by use of *Ci*). We propose that an areal or regional across-site calibration scheme that uses such 'regional' *Ci* can be particularly valuable when the main investigatory focus is on spatial variations of *Tss* rather than temporal *Tss* profiles at individual sites.

Supplement 2D describes why soil heat flow is not explicitly modeled for inclusion in model Eq. (9), instead site-mean soil heat flow is incorporated into fitted values of *C1* and C_h. There may be a less cumbersome approach to estimating soil heat flow than numerical modeling (e.g. force-restore, finite-element) which can be used for regions with a long duration snow-cover season, and which also might help enable temporally invariant regional calibration factors during the snow-free season (see Supplement 2D).

Like model Eq, (10), other *Ts* models have been used successfully in seasonal snow-cover areas without explicitly modeling physical effects of snow-cover or freeze/thaw on the surface energy balance (e.g. Krarti et al., 1995; Ouzzane et al., 2014; Badache et al., 2016). The brief episodes of soil freeze at some sites in the Tahoe study area did not discernably affect model Eq. (13) fit to the *Tss{an}* data at these sites (Section 4.2). However it would be of value to formulate a *Tss{an}* model with the property that calibration results for one year could be reliably extended to years with widely different snow-cover periods (see Section 4.5). Supplement 2F outlines one such scheme, which uses snow-cover date data for areas (such as the Tahoe study area) where *Tss* is usually near 0 °C during snow-cover periods.

5.2.3. Applicability of the soil T models, and soil T mapping

The ground surface energy flux and temperature models in Section 2 are applicable throughout most of the Sierra Nevada and other regions in the world, excluding permafrost areas. Supplement 2G outlines use of Eqs. (9) and (10) for *Tss* modeling of other regions, and for sub-monthly time periods.

By using Eqs. (9) or (10) to model *Tss*, maps of *Tss* over a landscape area can be simulated using data commonly available as GIS coverages: slope, aspect, elevation, leaf-area index (LAI) or other measure (e.g., NDVI) of vegetative cover density, and ground surface α and ε_g or soil color. In order to use LAI, the term *f* in Section 2 is replaced using the Beer-Lambert law expressing insolation attenuation in terms of LAI (e.g., Liang et al., 2013). In addition to *Tss* data for one seasonal or annual period for initial model calibration, time-dependent data or seasonal indices are needed for: (i) *Ta* (ii) insolation and/or seasonal cloud cover (iii) soil moisture and/or precipitation (and seasonal snow-cover, if present). Related *Ts* mappings have been reported (e.g., Kang et al., 2000; Signorelli and Kohl, 2004).

5.3. Two implications of observational and model results

5.3.1. Climate change influence on soil temperature

Multi-annual mean *Ts* at any location can shift as a consequence of changes in local vegetative cover or regional climate. Areal vegetation can change over decadal and longer time scales due to normal succession (e.g. recovery from timber harvesting or wildfires) in a stationary climate, or in response to climate change. Warming of ~1–2 °C has been documented for winter and annual mean *Ta* in the Sierra Nevada over the last few decades (Dettinger and Cayan, 1995; Dettinger, 2002; Barnett et al., 2008). Compilations of worldwide data indicate that trends in *Ts{an}* closely track trends in *Ta{an}* in many regions (Beltrami et al., 2000; Huang et al., 2000; Hu and Feng, 2003; Chapman et al., 2004).

However in some regions *Ts{an}* has warmed at a different rate than *Ta{an}* (see Knight et al., 2018) due to the influence of additional factors that affect the ground surface energy balance, such as seasonal snow-cover (e.g., Zhang, 2005; Qian et al., 2011). Shifts in (*Ts{an}-Ta{an}*) may have already occurred within the Sierra Nevada over the last several decades as a consequence of shorter duration of winter snow-cover due to *Ta* warming (e.g., Bartlett, 2001). The *z* dependence of *Tss{an}* in our study area suggests that currently in the Sierra Nevada at *z* lower than the Tahoe study area, and in the future throughout the Sierra Nevada as *Ta* warming causes the winter snow-cover period to become shorter, then

(i) the inter-site range of (*Ts{an}-Ta{an}*) may increase significantly (note calibrated negative value of lapse coefficient C_{Lr} in Table 3), since the seasonal snow-cover period during which all sites share a common *Tss* ~ 0 °C would be shorter. For example, in the Tahoe study area there was less snowfall and earlier spring melt during WY 2007 than WYs 2005 and 2006; WY 2007 also had the widest inter-site range of *Tss{an}*.
(ii) at exposed sites *Ts{an}* may warm faster than does *Ta{an}* and at forested sites *Ts{an}* may warm more slowly than *Ta{an}*. Areal-mean (*Ts{an}-Ta{an}*) changes may depend mainly on changes in areal vegetation density that could occur as regional *Ta{an}* warms.

For Canada, areal-mean *Ts{an}* during the 20th century warmed less than did *Ta{an}* (Zhang et al., 2005). At 30 sites across Canada, warming trends in spring and summer *Ts* were associated with *Ta* warming trends; however winter and annual *Ts* did not warm discernably due to winter snow-cover effects and snow-cover trends (Qian et al., 2011).

Results also have implications for interpretation of ground surface temperature histories (GSTH) reconstructed from borehole temperature-depth data (e.g. Beltrami, 2002). Results for Tahoe suggest that in seasonally snow-covered areas, *Tss{an}* may be especially sensitive to vegetative cover density and also to spring snowmelt timing. Therefore GSTH may be sensitive to even small shifts in vegetation density and to the timing of spring snowmelt completion that might accompany long-term changes in regional *Ta{an}*, such that GSTH is likely site-dependent with a complex relationship to regional climate history.

5.3.2. Soil temperature and groundwater flow tracing

Spatial variations in *Ts* or (*Ts-Ta*) have generally been neglected in thermal tracing investigations of groundwater flow for all but the shallowest of aquifers, presumably owing to lack of data for reliable estimates of (*Ts-Ta*) spatial variations. The presence of *Ts{an}* spatial heterogeneity across local to area scales can have a major influence on subsurface conductive heat flow to depths of ~ 250 m or more (e.g., Safanda, 1999; Kohl et al., 2001).

Tss findings and patterns pertinent to thermal tracing of groundwater flow include:

(i) Soil freezing did not occur at most sites during most cold seasons, and where it did occur was nearly always of short duration and small amplitude. This indicates that the thermal offset (decrease of *Tss{an}* with depth in the soil) is likely <0.3 °C (see Goodrich, 1982) at nearly all locations in the study area. Such small thermal offsets are negligible for determination of thermal boundary conditions in areal models of subsurface coupled heat and groundwater flow when focus is on areal groundwater flow below the

water table.

(ii) In the Tahoe study area, *Tss* > 0 °C during the entire period of spring snowmelt at all sites monitored for each of three WY. Therefor snowmelt infiltration in the South Tahoe valley area and nearby slopes at $z < \sim 2.4$ km is not typically impeded by frozen topsoil.

(iii) There can be very large spatial variations in *Ts{an}* within any narrow elevation band.

(iv) The *z* lapse of areal-mean *Ts{an}* can differ from lapse of free air or of *Ta{an}*.

(v) Groundwater recharge *T* (*Tr*) can be substantially different from mean areal *Ts* if recharge is spatially non-uniform (e.g., more recharge at cool densely vegetated drainage depressions).

(vi) Past or ongoing long-term *Ts{an}* changes (due, e.g., to past changes in vegetation and ongoing climate change) affect deeper subsurface *T*, and can obscure or complicate interpretation of the relationship of subsurface *T* to groundwater flow in shallow aquifers (Ferguson and Woodbury, 2005; Hendry and Woodbury, 2007; Trask and Fogg, 2009).

Accurate representation of major long-term temporal changes and of spatial variations of *Ts{an}* and *Tr* are needed as top surface thermal boundary conditions in order to reliably model coupled areal subsurface water and heat flow, particularly in mountain regions with large spatial variations in *Ts{an}*. This enables subsurface *T* variations (measured in wells and boreholes) caused by groundwater advection of heat to be distinguished from those caused by purely conductive heat flow. Factors (i) thru (vi) above are also pertinent to inference of groundwater recharge source areas using dissolved gas data. Supplement 6A reviews thermal tracing of groundwater flow, and supplement 6B outlines how to estimate and incorporate spatial *Ts{an}* variations in models of coupled groundwater and heat flow.

6. Summary and conclusions

Accurate *Tss* measurements were logged at numerous sites in the mountainous southern Tahoe Basin at thirty minute intervals for one to three years. Within an elevation band of just 0.02 km, widths of inter-site ranges of *Tss* data observations were 7.0 °C for WY 2007, 17.8 °C for July 2005, and 17.0 °C for Aug. 2005, which are each broader than the authors could find in any other published investigation. The large inter-site *Tss* variations are attributable to the great diversity of site conditions at which *Tss* were monitored, which are characteristic of the Sierra Nevada. In this mid-latitude sunny mountain region there are large spatial variations of (i) over-canopy solar radiation flux due to large contrasts in slope and aspect, as well as significant terrain shading in some valley floor locations, (ii) types and densities of vegetative cover. Factors (i) and (ii) together govern the intensity of solar flux incident on the ground surface, and affected Tahoe inter-site *Tss* variability much more than did inter-site variations in all other factors combined, including soil evaporation *E* and *Ta* lapse over a 0.41 km range of *z*. The relatively small influence of *E* on summer monthly and annual *Tss* is attributable to the montane Mediterranean climate: typically study area soils are snow-covered from Nov. to May, and from July thru Sept. are re-wetted only by sporadic thunderstorms. Perennially damp areas (in wet meadows) are mostly covered by lush grass; cool *Tss* here is attributable mainly to shading and secondarily to *E* and transpiration.

Two *Tgs* models are introduced, each developed from a ground surface energy flux balance. The models are formulated with site environmental parameters for which data or estimates are widely available, and with a few regional calibration coefficients. This article demonstrates that such physically based models can (a) accurately reflect the wide inter-site variations of *Tss* that occur at all times during the snow-free season(s) in an area/region with diverse ground surface environments, and (b) accurately reflect inter-site variations of mean annual *Tss* in areas with a long seasonal snow-cover period. Such models enable simulation of accurate gap-free maps of *Tss* over a heterogeneous landscape area or region at fine spatial resolution. The *Tss* models in this article could be refined with more thorough parameterization of energy balance terms or adjusted for use with snow-cover date data, possibly enabling even more accurate *Tss* output and extending the applicability of an annual *Tss* model calibration to years with significantly different snow-cover periods.

For montane and sub-alpine areas, our *Tss* observational and model findings also suggest spatially heterogeneous responses of local and areal *Ts{an}* to regional climate change, and underscore the importance of identifying spatial (and temporal) variations of *Ts{an}* for groundwater flow tracing using either heat flow or dissolved gas levels.

Declaration of Competing Interest

The authors declare that they have no known competing financial interests or personal relationships that could have appeared to influence the work reported in this paper.

Acknowledgements

Research was funded by: (1) The Division of Planning and Local Assistance of the California Department of Water Resources, through the Local Groundwater Management Assistance Act of 2000 (grant agreement No. 4600003173), and (2) The University of California Water Resources Center, for Project No. WR-1066: Investigation of Groundwater Flow in Foothill and Mountain regions using Heat Flow measurements.

Appendix A. Supplementary data

Supplementary data to this article can be found online at https://doi.org/10.1016/j.geoderma.2020.114202.

References

Allen, R.G., Trezza, R., Tasumi, M., 2006. Analytical integrated functions for daily solar radiation on slopes. Agric. For. Meteorol. 139, 55–73. https://doi.org/10.1016/j.agrformet.2006.05.012.

Badache, Messaoud, Eslami-Nejad, Parham, Ouzzane, Mohamed, Aidoun, Zine, 2016. A new modeling approach for improved ground temperature profile determination. Renew. Energy 85, 436–444. https://doi.org/10.1016/j.renene.2015.06.020.

Ballard, T.M., 1972. Subalpine soil temperature regimes in Southwestern British Columbia. Arct. Alp. Res. 4 (2), 139–146.

Barnett, T.P., Pierce, D.W., Hidalgo, H.G., Bonfils, C., Santer, B.D., Das, T., Bala, G., Wood, A.W., Nozawa, T., Mirin, A.A., Cayan, D.R., Dettinger, M.D., 2008. Human-induced changes in the hydrology of the Western United States. Science 319, 1080–1083. https://doi.org/10.1126/science 1152538.

Bartlett, M.G., 2001. Snow and the Ground Temperature Record of Climate Change, M.S. Thesis, University of Utah, Salt Lake City, UT.

Baxter, D.O., 1997. A comparison of deep soil temperature: Tennessee versus other locations. Trans. Am. Soc. of Agric. Engs. 40 (3), 727–738.

Beltrami, H., Wang, J.F., Bras, R.L., 2000. Energy balance at the Earth's surface: heat flux history in eastern Canada. Geophys. Res. Lett. 27 (20), 3385–3388. https://doi.org/10.1029/2000GL008483.

Beltrami, Hugo, 2002. Earth's long-term memory. Science 297 (5579), 206–207.

Birkeland, P.W., 1964. Pleistocene glaciation of the Northern Sierra Nevada, North of Lake Tahoe, California. J. Geol. 72 (6), 10–25.

Brearshears, D.D., Nyhan, J.W., Heil, C.E., Wilcox, B.P., 1998. Effects of woody plants on microclimate in a Semiarid Woodland: soil temperature and evaporation in canopy and intercanopy patches. Int. J. Plant Sci. 159 (6), 1010–1017.

Brutsaert, W., 1975. On a derivable formula for long-wave radiation from clear skys. Water Resour. Res. 11, 742–744.

Chapman, D.S., Chisholm, T.J., Harris, R.N., 1992. Combining borehole temperature and meteorologic data to constrain past climate change. Palaeogeogr. Palaeoclimatol. Palaeoecol. (Glob. Planet. Chang. Section) 98, 269–281.

Chapman, D.S., Bartlett, M.B., Harris, R.N., 2004. Comment on "Ground vs. surface air temperature trends: implications for borehole surface temperature reconstructions" by M.E. Mann and G. Schmidt. Geophys. Res. Lett.:Clim. 31 (7). https://doi.org/10.1029/2003GL019054. L07205.

Clinton, B.D., 2003. Light, temperature, and soil moisture responses to elevation, evergreen understory, and small canopy gaps in the southern Appalachians. For. Ecol. Mgemt. 186 (1–3), 243–255. https://doi.org/10.1016/S0378-1127(03)00277-9.

Coops, N.C., Waring, R.H., Moncrieff, J.B., 2000. Estimating mean monthly incident solar radiation on horizontal and inclined slopes from mean monthly temperature extremes. Int. J. Biometeor. 44 (4), 204–211. https://doi.org/10.1007/s004840000073.

Crippen, J.R., Pavelka, B.R., 1970. The Lake Tahoe Basin, California-Nevada. United States Geological Survey, Water-Supply Paper No. 1972.

Deardorff, J.W., 1978. Efficient prediction of ground surface temperature and moisture, with inclusion of a layer of vegetation. J. Geophys. Res. 83 (C4) Paper No. 7C0816.

Dettinger, M.D., Cayan, D.R., 1995. Large-scale atmospheric forcing of recent trends toward early snowmelt runoff in California. J. Clim. 8, 606–623.

Dettinger, M., 2002. Responses of Sierra Nevada Resources to future climate changes. Sierra Nevada Science Symposium, Oct. 7–10, University of California and United States Forest Service, Kings Beach, California.

Dingman, L.S., 2002. Physical Hydrology, second ed. Prentice Hall, New Jersey.

Dobrowski, S.Z., Abatzoglou, J.T., Greenberg, J.A., Schladow, S.G., 2009. How much influence does landscape-scale physiography have on air temperature in a mountain environment? Agric. For. Meteorol. 149, 1751–1758. https://doi.org/10.1016/j.agrformet.2009.06.006.

Ferguson, G., Woodbury, A.D., 2005. The effects of climatic variability on estimates of recharge from temperature profiles. Ground Water 43 (6), 837–842. https://doi.org/10.1111/j.1745-6584.2005.00088.x.

Freeman, Gary J., 2009. Diminishing snowfall in central and northern California's mixed rain and snow elevational zone. In: Paper presented at Western Snow Conference 2009, gif2@pge.com.

Garcia-Suarez, A.M., Butler, C.J., 2006. Soil temperatures at Armagh observatory, Northern Ireland, from 1904 to 2002. Int. J. Climatol. 26 (8), 1075–1089. https://doi.org/10.1002/joc.1294.

Goodrich, L.E., 1982. The influence of snow cover on the ground thermal regime. Can. Geotech. J. 19, 421–432.

Graham, E.A., et al., 2012. Fine scale patterns of soil and plant surface temperatures in an alpine fellfield habitat, White Mountains, California. Arct. Antarc. Alp. Res. 44 (3), 288–295. https://doi.org/10.1657/1938-4246-44.3.288.

Hatchett, Benjamin J., Daudert, Britta, Garner, Christopher B., Oakley, Nina S., Putnam, Aaron E., White, Alan B., 2017. Winter snow level rise in the Northern Sierra Nevada from 2008 to 2017. Water 9 (899). https://doi.org/10.3390/w9110899.

Hendry, M.J., Woodbury, A.D., 2007. Clay aquitards as archives of holocene paleoclimate: $d^{18}O$ and thermal profiling. Ground Water 45 (6), 683–691. https://doi.org/10.1111/j.1745-6584.2007.00354.x.

Herb, William R., Janke, Ben, Mohensi, Omid, Stefan, Heinz G., 2008. Ground surface temperature simulation for different land covers. J. Hydrol. 356, 327–343. https://doi.org/10.1016/j.jhydrol.2008.04.020.

Hu, Q., Feng, S., 2003. A daily soil temperature dataset and soil temperature climatology of the contiguous United States. J. Appl. Meteorol. 42 (8), 1139–1156. https://doi.org/10.1175/1520-0450(2003)042<1139:ADSTDA>2.0.CO;2.

Huang, S., Pollack, H.N., Shen, P., 2000. Temperature trends over the past five centuries reconstructed from borehole temperatures. Nature 403 (6771), 756–758. https://doi.org/10.1038/35001556.

Jimenez, C., Tejedor, M., Rodriguez, M., 2007. Influence of land use changes on the soil temperature regime of Andesols on Tenerife, Canary Islands, Spain. Eur. J. Soil Sci. 58 (2), 445–449. https://doi.org/10.1111/j.1365-2389.2007.00897.x.

Jin, M., 2004. Analysis of land skin temperature using AVHRR observations. Bull. Am. Meteorol. Soc. 85 (4), 587–600. https://doi.org/10.1175/BAMS-85-4-587.

Jury, W.A., Gardner, W.R., Gardner, W.H., 1991. Soil Physics, fifth ed. John Wiley & Sons Inc, New York.

Kang, S., Kim, S., Oh, S., Lee, D., 2000. Predicting spatial and temoporal patterns of soil temperature based on topography, surface cover and air temperature. For. Ecol. Mgemt. 136, 173–184.

Knight, J.H., Minasny, B., McBratney, A.B., Koen, T.B., Murphy, B.W., 2018. Soil temperature increase in eastern Australia for the past 50 years. Geoderma 313, 241–249. https://doi.org/10.1016/j.geoderma.2017.11.015.

Kohl, T., Signorelli, S., Rybach, L., 2001. Three-dimensional (3-D) thermal investigation below high Alpine topography. Phys. Earth Planet. Interiors 126 (3–4), 195–210.

Krarti, M., Lopez-Alonso, C., Claridge, D.E., Kreider, J.F., 1995. Analytical model to predict annual soil surface temperature variation. J. Solar Energy Eng. 117 (91).

Kunkel, V., Wells, T., Hancock, G.R., 2016. Soil temperature dynamics at the catchment scale. Geoderma 273, 32–44. https://doi.org/10.1016/j.geoderma.2016.03.011.

Kustas, W.P., Rango, A., Uijlenhoet, R., 1994. A simple energy budget algorithm for the snowmelt runoff model. Water Resour. Res. 30, 1515–1527.

Liang, L.L., Riveros-Ireguil, D.A., Emanuel, R.E., McGlynn, B.L., 2013. A simple framework to estimate distributed soil temperature from discrete air temperature measurements in data-scarce regions. J. Geophys. Res. Atmos. 119 (2), 407–417. https://doi.org/10.1002/2013JD020597.

Lin, J.D., 1980. On the force-restore method for prediction of ground surface temperature. J. Geophys. Res. 83 (C6), 3252–3254 Paper No. 80C0236.

Liu, X., Luo, T., 2011. Spatiotemporal variability of soil temperature and moisture across two contrasting timberline ecotones in the Sergyenia Mountains, Southeast Tibet. Arct. Antarct. Alp. Res. 43 (2), 229–238. https://doi.org/10.1657/1938-4246-43.2.229.

Maurer, Gregory E., Bowling, David R., 2014. Seasonal snowpack characteristics influence soil temperature and water content at multiple scales in interior western U.S. mountain ecosystems. Water Resour. Res. 50, 5216–5234. https://doi.org/10.1002/2013WR014452.

Mihalakakou, G., Santamouris, M., Lewis, J.O., Asimakopoulos, D.N., 1997. On the application of the energy balance equation to predict ground temperature profiles. Solar Energy 60 (3/4), 181–190.

Minder, Justin R., Kingsmill, David E., 2013. Mesoscale variations of the atmospheric snow line over the Northern Sierra Nevada: multiyear statistics, case study, and mechanisms. J. Atm. Sci. 70. https://doi.org/10.1175/JAS-D-12-0194.1.

NRCS and NWCC, 2005. Snowpack telemetry and snow course data, including for the Tahoe Basin for winter 2004-2005. Link: https://www.wcc.nrcs.usda.gov/snow/ (accessed 30 Nov. 2018).

Oku, Y., Ishikawa, H., Haginoya, S., Ma, Y., 2006. Recent trends in land surface temperature on the Tibetan Plateau. J. Clim. 19 (12), 2995–3003. https://doi.org/10.1175/JCLI3811.1.

Oliva, M., Ortiz, A.G., Salvador, F., Salva, M., Pereira, P., Geraldes, M., 2014. Long-term soil temperature dynamics in the Sierra Nevada, Spain. Geoderma 235–236, 170181. https://doi.org/10.1016/j.geoderma.2014.07.012.

Ouzzane, Mohamed, Elsami-Nejad, Parham, Aidoun, Zine, Lamarche, Louis, 2014. Analysis of the convective heat exchange effect on the undisturbed ground temperature. Solar Energy 108, 340–347. https://doi.org/10.1016/j.solener.2014.07.015.

Paul, Keryn I., Polglase, Philip J., Smethurst, Philip J., O'Connell, Anthony M., Carlyle, Clive J., Khanna, Partap K., 2004. Soil temperature under forests: a simple model for predicting soil temperatures under a range of forest types. Agric. For. Meteorol. 121, 167–182. https://doi.org/10.1016/j.agrformet.2003.08.030.

Qian, B., Gregorich, E.G., Gameda, S., Hopkins, D.W., 2011. Observed soil temperature trends associated with climate change in Canada. J. Geophys. Res. 116https://doi.org/10.1029/2010JD015012. Article D02106.

Quan, J., Zhan, W., Ma, T., Du, Y., Guo, Z., Qin, B., 2018. An integrated model for developing hourly Landsat-like land surface temperatures over heterogeneous landscapes. Rem. Sens. Env. 206, 403–423. https://doi.org/10.1016/j.rse.2017.12.003.

Rajver, D., Safanda, J., Dedecek, P., 2006. Monitoring of air-ground temperature coupling and examples of shallow subsurface warming in Slovenia. Geologija 49 (2), 279–293.

Raub, W., Brown, C.S., and Post, A., 2006. Inventory of Glaciers in the Sierra Nevada, California: U.S. Geological Survey Open-File Report 2006-1239. 232 p. (online only).

Safanda, J., 1999. Ground surface temperature as a function of slope angle and slope orientation and its effect on the subsurface temperature field. Tectonophysics 306 (3–4), 367–375. https://doi.org/10.1016/S0040-1951(99)00066-9.

Signorelli, S., Kohl, T., 2004. Regional ground surface temperature mapping from meteorological data. Glob. Planet. Chang. 40 (3), 267–284.

Taniguchi, M., Williamson, D.R., Peck, A.J., 1999. Disturbances of temperature-depth profiles due to surface climate change and subsurface water flow: 2. An effect of step increase in surface temperature caused by forest clearing in southwest Western Australia. Water Resour. Res. 35 (5), 1519–1529.

Thodal, C.E., 1997. Hydrogeology of Lake Tahoe Basin, California and Nevada, and Results of a Ground-Water Quality Monitoring Network, Water Years 1990-92. U. S. Geological Survey, Water-Resources Investigations Report 97-4072.

Trask, J.C., Fogg, G.E., 2009. Investigation of Groundwater Flow in Foothill and Mountain regions using Heat Flow measurements. University of California Water Resources Center, Technical Completion Report Project No. WR-1006. Permalink: https://escholarship.org/uc/item/73r8k2q4 (accessed 16 Nov. 2018).

USDA and NRCS, 2007. Soil Survey of the Tahoe Basin, California and Nevada. U.S. Dept. of Agricul. Link: (accessed 17 Nov. 2018): https://www.nrcs.usda.gov/wps/portal/nrcs/soilsurvey/soils/survey/state/.

West, E.S., 1952. A study of the annual soil temperature wave. Aust. J. Sci. Res. Series A: Phys. Sci. 5, 303–314.

Wundram, D., Pape, R., Loffler, J., 2010. Alpine soil temperature variability at multiple scales. Arct. Antarct. Alp. Res. 42 (1), 117–128. https://doi.org/10.1657/1938-4246-42.1.117.

Zhang, T., 2005. Influence of the seasonal snow cover on the ground thermal regime: an overview. Rev. Geophys. 43 (4). https://doi.org/10.1029/2004RG000157. Article RG4002.

Zhang, Y., Chen, W., Smith, S.L., Riseborough, D.W., Cihlar, J., 2005. Soil temperature in Canada during the twentieth century: Complex responses to atmospheric climate change. J. Geophys. Res. 110https://doi.org/10.1029/2004JD004910. Article D03112.